Simulation of a Progressive Derecho Using Composite Initial Conditions

MICHAEL C. CONIGLIO

School of Meteorology, University of Oklahoma, and Cooperative Institute for Mesoscale Meteorological Studies, Norman, Oklahoma

DAVID J. STENSRUD

NOAA/National Severe Storms Laboratory, Norman, Oklahoma

(Manuscript received 4 August 1999, in final form 15 November 2000)

ABSTRACT

This study focuses on the progressive derecho, a widespread, convectively induced windstorm produced by a mesoscale convective system that often occurs within a relatively benign synoptic-scale environment. Sounding data from 12 progressive derechos, which occurred in weakly forced large-scale environments, are composited in order to examine important large-scale features in the preconvective environment. This analysis captures many features that are common in warm season derecho environments, such as an upper-level wind maximum, a relatively dry midtroposphere, and low-level warm advection. Initial and boundary conditions for the Pennsylvania State University–National Center for Atmospheric Research fifth-generation Mesoscale Model (MM5) are created using this analysis. A three-dimensional, horizontally nonhomogeneous, explicitly resolved simulation of a progressive derecho is produced and compared to previous, more idealized simulations of similar convective systems that have been used to explain the strength and structure of observed long-lived squall lines and bow echoes.

A subset of previous squall line simulations produced within horizontally homogeneous environments without wind shear above 5 km suggests that a balance between the positive vorticity associated with the environmental low-level shear (Δu) and the negative vorticity created baroclinically at the leading edge of the cold pool (C) is the essential ingredient that determines the strength and time-dependent structure of long-lived squall lines (local balance theory). In the simulation presented here, which occurs in an environment with deep-tropospheric shear but relatively weak low-level shear, the model develops a realistic, rapidly moving squall line with embedded bow echoes that maintains its strength for much longer than the squall lines within previous idealized simulations that develop and evolve within similar less than optimal balance conditions ($C/\Delta u > 2$). Previous simulations of squall lines under similar less than optimal conditions contain updrafts that progressively weaken and become more upshear tilted with time as the cold pool surges ahead of the updrafts within 1–3 h after the system develops. However, the simulated squall line used here contains convective updrafts that remain almost directly above the gust front, maintains a nearly constant upshear tilt for several hours, and produces severe, near-surface winds for over 8 h. Examination of the maximum grid-resolved vertical velocity indicates that the cells are not weakening with time relative to their thermodynamic potential, which contrasts the behavior of the cells within the less than optimal squall lines of the previous, idealized simulations.

These results support the idea that local balance theory, which attempts to explain both the strength and longevity of squall lines, may be incomplete within environments that often favor warm season progressive derechos. In particular, tests with a simple two-dimensional cloud-scale model indicate that both significant upper-tropospheric shear above 5 km (which is found in the composite analysis and in the MM5 solution) and low-level shear play significant roles in maintaining the strength of squall lines over long periods and need to be considered in order to fully understand and forecast these events.

1. Introduction

Strong, horizontal surface winds associated with convection are almost always the result of intense thunderstorm downdrafts. The main source of downward motion within thunderstorms is the negative buoyancy of air parcels resulting from evaporation and/or the melting and sublimation of frozen precipitation as it falls through subsaturated air (Johns and Doswell 1992). As the convection organizes and grows in size, the downdrafts accumulate to form a pool of cold air and an associated region of hydrostatically induced high pressure (a mesohigh) (Fujita 1955). The most concentrated leading edge of this cold pool is referred to as the gust front, which contains a wind surge behind the leading edge that can often exceed severe limits (>26 m s^{-1}) (Wakimoto 1982). Fujita (1976) identifies intense downdrafts of air, called downbursts, that induce an outburst of highly divergent, damaging winds on or near the

Corresponding author address: Michael C. Coniglio, National Severe Storms Laboratory, 1313 Halley Circle, Norman, OK 73069.
E-mail: Mike.Coniglio@nssl.noaa.gov

ground. These damaging winds associated with downbursts and the gust front are often termed straight-line winds to distinguish them from the twisting nature of the damage produced by tornadoes (Fujita 1981). Straight-line winds can be as destructive as tornadoes while often covering larger geographical areas (Fujita 1981; Fujita and Wakimoto 1981; Johns and Hirt 1985; Przybylinski 1995).

Hinrichs (1888) describes a type of widespread, convectively induced windstorm, which he terms a derecho (a Spanish word for ''straight ahead'' or ''direct''). Overshadowed by the tornado's more visually dynamic and devastating nature, derechos received little attention in the scientific literature for many decades. Almost a century later, Johns and Hirt (1987, hereafter JH87) define the derecho to include any family of downburst clusters [a concentrated area of severe wind reports and/or wind damage with a major axis length of at least 400 km; Fujita and Wakimoto (1981)] associated with an extratropical mesoscale convective weather system (MCS) (Maddox 1980a; Houze et al. 1989). A *serial* derecho is produced by several separate convective elements and is favored under strong large-scale forcing, and a *progressive* derecho is produced by a single, curved squall line or MCS oriented perpendicular to, and with a bulge in the general direction of, the mean midtropospheric flow. Fujita (1978), following the work of Nolan (1959) and Hamilton (1970), refers to a bulging convective line as a ''bow echo'' and shows that strong, diverging outflow and associated swaths of damaging surface winds are often found near the apex of the bow. Przybylinski and DeCaire (1985) show that channels of weak radar reflectivity behind the leading edge of the convective line often precede the development of a bow echo and are proposed to be associated with strong rear-inflow and intense downdrafts of evaporatively cooled air. These features often exist on many different scales within a derecho-producing MCS and may be present simultaneously during a single event (Johns and Doswell 1992; Przybylinski 1995).

In the United States, derechos are generally restricted to the states east of the Rocky Mountains and occur most frequently in the southern and central plains and the Ohio valley during the summer months (JH87; Bentley and Mote 1998). Warm season derechos tend to occur in environments with large convective instability, strong midtropospheric winds, and a dry mean midtroposphere, with many occurring with a weak to nonexistent 500-hPa short-wave trough (JH87). In addition, low-level warm advection, pooling of very high dewpoints along a low-level quasi-stationary frontal boundary, and a poleward jet maximum along the northern periphery of an upper-level ridge are often found in the large-scale environment (Johns 1984; JH87; Johns et al. 1990, hereafter J90; Johns 1993).

The important local-scale mechanisms that determine the strength and structure of long-lived squall lines, of which derecho-producing MCSs are a subset, have been examined through highly idealized numerical simulations (Thorpe et al. 1982; Fovell and Ogura 1988; Rotunno et al. 1988, hereafter RKW88; Weisman et al. 1988, hereafter WKR88; Weisman 1992, hereafter W92; Skamarock et al. 1994). In particular, RKW88, WKR88, and W92 use results from 2D and 3D cloud-resolving numerical simulations to develop a local balance theory for strong, long-lived squall lines. The model simulations are initialized with horizontally homogeneous environments consisting of a relatively moist and unstable environment with the total shear restricted to the lower troposphere. RKW88 find that within their idealized framework, the essential ingredient that sustains a long-lived squall line is an amount of low-level shear that counters the circulation induced by the convectively generated cold pool. This conclusion is further strengthened in Rotunno et al. (1990) where an appropriate balance between the environmental low-level shear and the cold pool is deemed a necessary condition for sustaining most strong, long-lived squall lines. An optimal state exists when the negative vorticity produced by the cold pool is balanced by the positive vorticity associated with the ambient low-level shear. Under these conditions, strong, vertically oriented convective cells are periodically generated directly above the gust front. For a given cold pool strength, values of low-level shear that are too large cause the convection to tilt downshear and cut off the supply of warm, moist air to the updraft (the ''greater than optimal'' condition). Values of low-level shear too small cause the updrafts to become weaker and tilted in the upshear direction (the ''less than optimal'' condition). Most of the simulations presented in RKW88 and WKR88 eventually reach the less than optimal state as the cold pool becomes colder with time, regardless of the initial conditions (the simulations with stronger low-level shear take longer to reach less than optimal conditions). In this manner, the less than optimal phase of the squall line life cycle is also viewed as a decaying phase as the system tilts more upshear with time and the gust front surges ahead of the updrafts.

W92 and Weisman (1993, hereafter W93) show that this theory can be modified to include the presence of rear inflow within the cold pool and to describe the genesis of idealized, long-lived bow echoes. W92, W93, and Weisman and Davis (1998) present idealized simulations where many of the observed, storm-scale structures of severe, long-lived squall lines and bow echoes are reproduced, including elevated rear-inflow jets and midlevel vorticity centers along the ends of the convective lines. These features develop during the less than optimal state as a response to the warm updraft air spreading rearward above the strengthening cold pool. W92 shows that squall lines that develop within sufficiently strong ambient low-level shear tend to develop elevated rear-inflow jets that help bring the systems back to a steady, nearly optimal state as they provide a source of positive vorticity within the cold pool.

In terms of the minimum ambient shear required to

simulate long-lived damaging wind events, W93 states that ''if we consider maximum 350-m winds of 35 m s^{-1} or greater as indicating significant potential for producing damaging surface winds, then we note that such systems occur for all cases of convective available potential energy (CAPE) greater than 2000 m^2 s^{-2} and shears greater than 15 m s^{-1} (over the lowest 2.5 or 5 km), including but not restricted to the cases that have evolved into structures similar to the idealized bow echo.'' (p. 666 of W93). Well-defined, long-lived bow echoes in the simulations of W93 require similar CAPE but at least 20 m s^{-1} of shear in the lower troposphere. Structures that produce these stronger near-surface winds are particularly favored if the total shear is confined to the lowest 2.5 km.

Despite much attention given to the environmental low-level shear associated with squall lines, there have been few detailed examinations of observed wind profiles in the vicinity of derechos. Bluestein and Jain (1985) develop a composite hodograph of four types of severe springtime squall lines in Oklahoma and generally find a kinematic environment with moderate-to-strong low-level directional shear with weaker shear aloft. However, since the springtime months often favor strong large-scale forcing for severe weather in the southern plains (Johns and Doswell 1992), these results are likely unrepresentative of the warm-season, weakly forced, progressive derecho. This is the type likely to be most relevant to the isolation of local-scale forcing within the numerical simulations of W93. Bentley et al. (1998) produce a composite hodograph taken near the initiation of 10 north-central Great Plains derecho events. They find moderate low-level directional shear with unidirectional shear above 3000 m above mean sea level (MSL). In a more comprehensive analysis, Evans and Doswell (1998, 2001) examine derecho environments using 113 proximity soundings. They find that, while derechos occur in environments with stronger lower-tropospheric shear than nonderecho events, the middle 50% of the distribution of 0–2- (0–6-) km shear vector magnitudes falls between 8 and 16 (11.75 and 20) m s^{-1} for all derecho events. For the weakly forced events, this same distribution for the 0–2- (0–6-) km shear vector magnitudes falls between 7 and 12 (10.5 and 20) m s^{-1}. This study shows that a significant number of derecho events appear to occur in environments below the minimum shear threshold suggested by the idealized simulations of W93 for producing a long-lived, damaging wind event.

The climatological study by Evans and Doswell (1998, 2000, manuscript submitted to *Wea. Forecasting*) emphasizes our lack of a complete dynamical understanding of the mechanisms that play a major role in determining the convective type, organization, and longevity of derechos. While RKW88, WKR88, W92, W93, Skamarock et al. (1994), and Weisman and Davis (1998) add valuable insight into the organization of squall lines and bow echoes, these simulations use an idealized horizontally homogeneous initial condition in which the wind shear is restricted to the lower troposphere. Although RKW88 and W93 compare a few observed cases with the results from local balance theory, the extent to which the local vorticity balance arguments can be used to explain the strength and longevity of a realistic, 3D progressive derecho event remains largely unresolved. Therefore, this study attempts to create a realistic simulation of a derecho-producing MCS from a numerical model that uses more realistic initial conditions and physical parameterization schemes than previous studies. This idealized, yet realistic, simulation acts as a surrogate for detailed observations of a typical progressive derecho event.

It is stressed that the objective of this modeling study is not to generalize the important mechanisms of derecho strength, structure, and longevity through comprehensive sensitivity studies. Instead, we examine how well the behavior of the simulated derecho-producing MCS, which develops in a mean environment typical of weakly forced derechos, compares to the aforementioned idealized simulations of strong, long-lived squall lines and bow echoes. These results may be useful in future observational field programs that attempt to provide the observations necessary to determine the mechanisms responsible for squall line and bow echo strength and structure. Section 2 summarizes the composite technique used to define the model initial and boundary conditions, and identifies the important large-scale features associated with derecho development. Section 3 summarizes the model configuration used, highlights the ability of the model to reproduce the preconvective environment found in the composite analysis, and shows that the simulated derecho reproduces many of the features seen in observational studies. Section 4 examines the extent to which the simulation agrees with the past simulations and presents some relevant 2D simulations. A final discussion is found in section 5.

2. Composite analysis

We begin by creating a realistic, horizontally nonhomogeneous initial condition using sounding data (0000 and 1200 UTC) from 12 warm season progressive derecho events that occurred in similar weakly forced, large-scale environments. In general, all derecho events that exhibit the dynamic pattern discussed by Johns (1993) are discarded; that is, if the convection occurs in direct association with a strong midlevel traveling wave disturbance and a significant surface cold front, the case is ignored. Although the selection of only weakly forced, warm season events eliminates some of the stronger sheared environments, these events are chosen to allow for a suitable comparison with previous idealized studies, which do not explicitly include strong, large-scale forcing.

A composite analysis of the conditions approximately 12 h prior to (t_o − 12 analysis), around (t_o − 0 analysis),

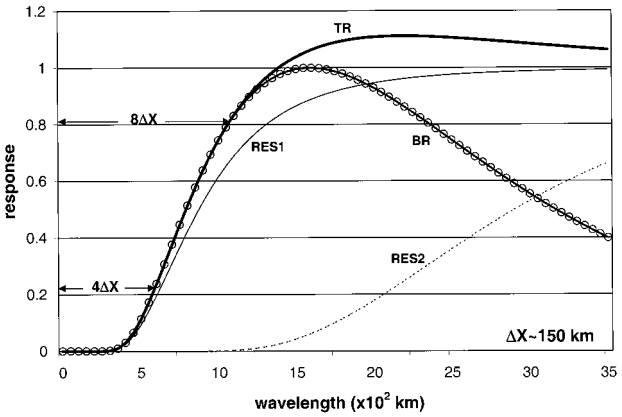

FIG. 1. Response curves for the analyses used in the scale separation technique. RES1 and RES2 represent the standard low-pass analyses, BR represents the bandpass analysis, TR is the response for the total meteorological field, and ΔX is the approximate average station spacing.

and 12 h after (t_o + 12 analysis) the time of MCS initiation is performed. The t_o − 12 and t_o + 12 analyses are valid at 1200 UTC, and the t_o − 0 analysis is valid at 0000 UTC. The location of each MCS initiation is positioned at the center of a 3000 km × 3000 km grid for all three analyses. The abscissa (x axis) of the grid is aligned with the direction of propagation of the MCS. The sounding locations with respect to the position of the MCS initiation and movement are then mapped onto the common grid for each of the 12 cases and for each analysis. The result gives a horizontal resolution of radiosonde measurements far greater than that available for an individual derecho case (each analysis contains about 600 observations with an average station spacing of about 150 km).

An objective analysis routine developed by Barnes (1973) is used to analyze the data at 20-km horizontal intervals[1] within the grid, and every 25 mb from the surface to 100 mb, creating a total of 151 grid points in each horizontal direction, and 37 pressure levels in the vertical. Following Maddox (1980b), two separate, low-pass analyses are used to create a bandpass analysis that maximizes details at a desired mesoscale wavelength range (Fig. 1). The appropriate analysis constants are chosen such that the low-pass field (RES2) represents the macroscale environment and the bandpass field (BR) represents the mesoscale perturbation. The bandpass response is maximized at a wavelength of 1600 km, which is similar to the value used by Maddox (1983) in a composite study of mesoscale convective complexes. The total meteorological field (TR) is then represented by the sum of the bandpass and low-pass objective analyses. The total response function associated with this field is greater than one due to a slight amplification imposed on the bandpass field (Maddox 1980b). Notice that the total response curve is steeper than the response curve from that of a standard low-pass analysis (RES1). As a result, the analysis suppresses most of the small-scale noise, yet retains a significant portion of waves greater than 1000 km, which is within the meso-α-scale range (Orlanski 1975).

The t_o − 0 composite analysis (Fig. 2) compares favorably to the composite results of JH87 and J90. Significant low-level warm advection and pooling of moisture along the derecho track is evident in the 850-hPa composite analysis (Fig. 2a). In addition, progressively weaker warm advection along the derecho track and large dewpoint depressions near and upstream from the composite MCS initiation region are seen in the 700-hPa composite analysis (Fig. 2b). The MCS initiation is positioned near a midlevel ridge axis (Fig. 2c) and in the vicinity of a 200-hPa jet with progressively weaker winds along the track (Fig. 2d), in agreement with the results of J90 and the analysis presented in Johns (1993).

3. Derecho simulation

The previous section shows that the composite method produces a realistic, nonhomogeneous, large-scale environment typical of a weakly forced derecho event. The next step is to use these analyses as initial and boundary conditions for the numerical model. The model chosen for use is the Pennsylvania State University–National Center for Atmospheric Research fifth-generation Mesoscale Model (MM5) (Dudhia 1993).

a. MM5 configuration

The domain configuration and the choice of model physics are summarized in Fig. 3. As mentioned previously, the composite analysis is performed on a grid with 20-km horizontal grid spacing. The coarse grid (grid 1) has identical horizontal dimensions as the analysis grid, giving 151 grid points in each direction with 20-km horizontal resolution. Thirty-five vertical sigma (σ) levels are used throughout the simulation. Grid 1 is initialized with the t_o − 12 analysis, providing a composite of the large-scale conditions at 1200 UTC (12 h prior to MCS initiation) and a 12-h model simulation is produced. Boundary conditions are provided by the successive composite analyses.

Once the model integration reaches 12 h (0000 UTC), two additional computational grids are introduced that use a two-way interactive nesting procedure. Grid 2 uses a 6.67-km horizontal resolution and is initialized with data from grid 1. There are 151 grid points in the x direction (1007 km) and 85 grid points in the y direction (567 km). The innermost grid (grid 3) uses a 2.22-km horizontal resolution and is initialized with data from grid 2. There are 136 grid points in each direction, giv-

[1] Although this small grid length is not justified by the data spacing, it is chosen to allow the development of mesoscale features in the model.

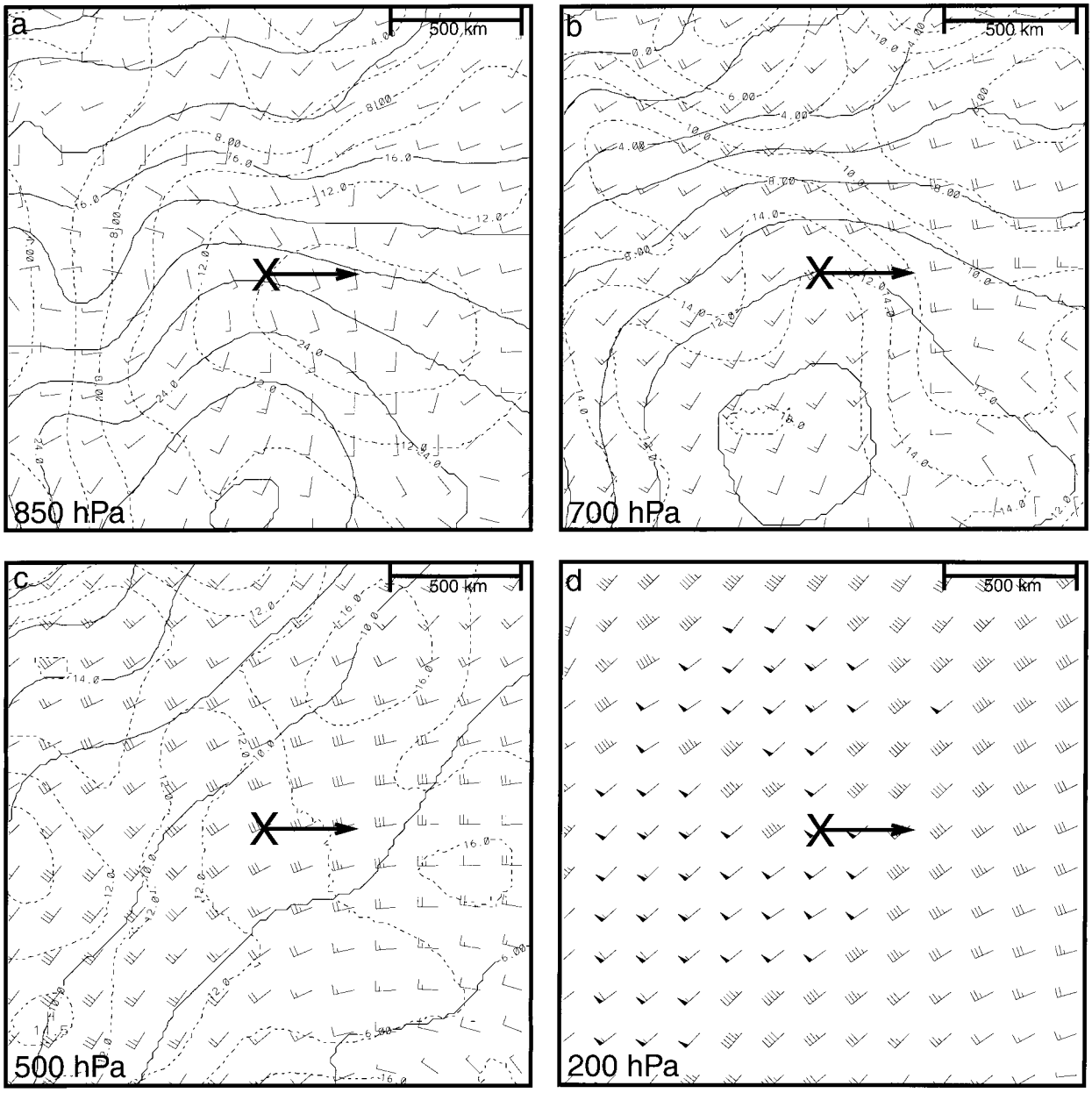

FIG. 2. Results from the t_o-0 composite analysis for (a) 850-hPa temperature (solid, every 2°C), dewpoint (dashed, every 2°C), and winds (full barb = 5 ms^{-1}), (b) as in (a) except at 700 hPa and dashed lines of dewpoint depression (every 2°C), (c) as in (b) except at 500 hPa, and (d) as in (b) except for winds only (flag = 25 m s^{-1}) at 200 hPa. The × denotes the location of the composite MCS initiation and the arrow points in the direction of the composite MCS movement. Only the central 2000 km × 2000 km portion of the analysis domain is shown.

ing dimensions of 300 km × 300 km. As the convection increases in size, a total of two inner grids are used and moved discretely so that the convection remains near the center of the grid. The model physics used on grids 2 and 3 are the same as those on the coarse grid except that the convective forcing is provided by the microphysical scheme alone, such that cumulonimbus clouds, and the direct convective feedbacks, are fully represented (Weisman et al. 1997).

b. Preconvective environment

The model solution at 12 h (0000 UTC) largely resembles the composite analysis valid at the same time. Several of the important features in the composite analysis and in J90 are in the model solution, including a quasi-stationary E–W frontal boundary at the surface (Fig. 4), deep pooling of moisture in low levels, relatively dry air in midlevels, a midlevel ridge axis near

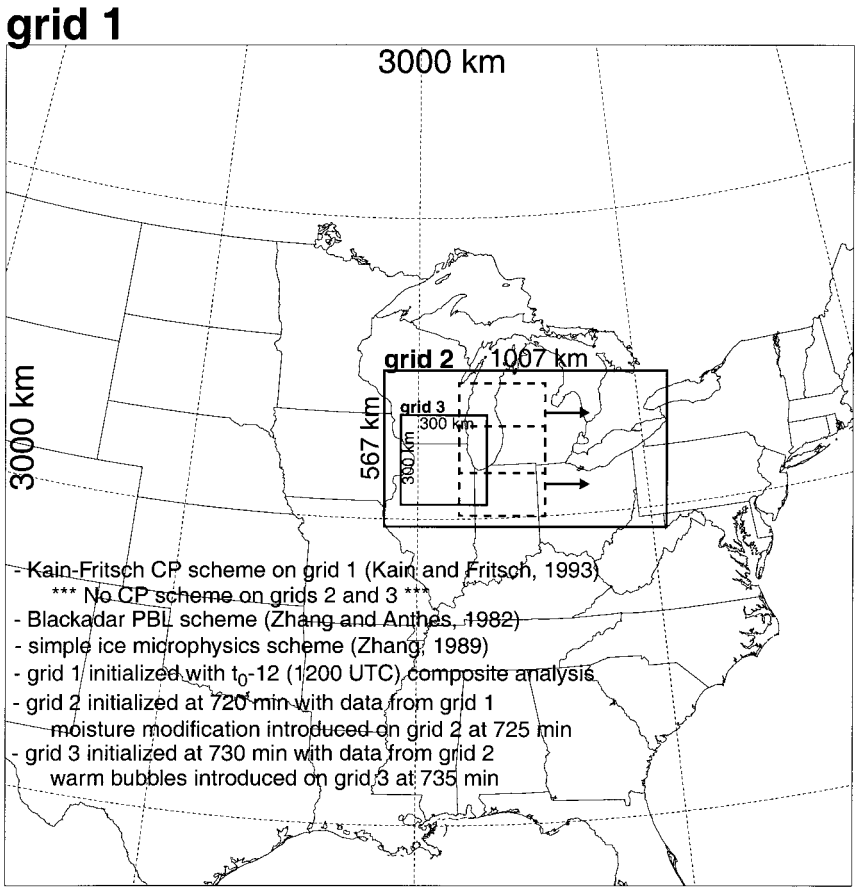

FIG. 3. Summary of the MM5 configuration. Grids 1, 2, and 3 use a 20-, 6.67-, and 2.22-km horizontal resolution, respectively. Each grid uses 35 vertical sigma levels. The dashed grids indicate the introduction of two separate inner grids so that the convective system is completely resolved at 2.22-km resolution. These grids are then moved with the system in the direction shown by the arrows. The map background is included on the grids to provide a scale reference.

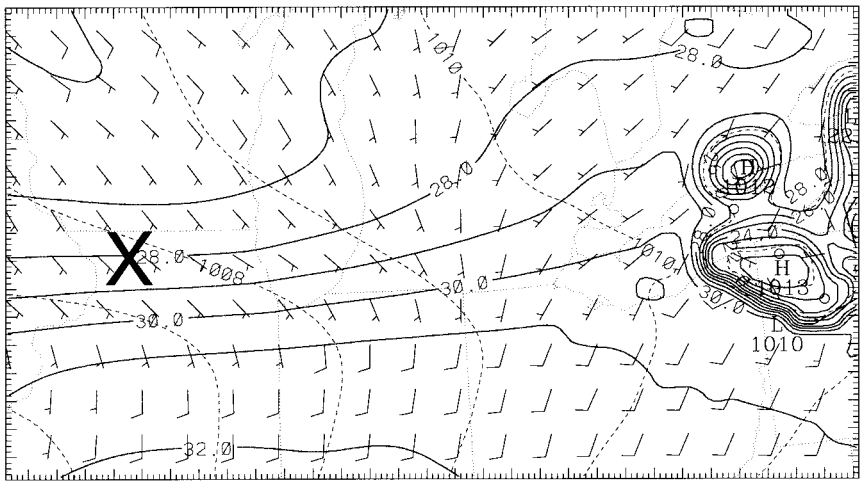

FIG. 4. MM5 solution displayed on grid 2 at the time grid 2 is initialized (12 h) of surface temperature (solid, every 1°C), sea level pressure (dashed, every 1 mb), and surface winds (plotted every eight grid points with full barb = 5 m s^{-1}). Tick marks are every 6.67 km. The × denotes the location of the composite MCS initiation. The feature on the far right is produced by parameterized convection on grid 1 prior to the initialization of grid 2.

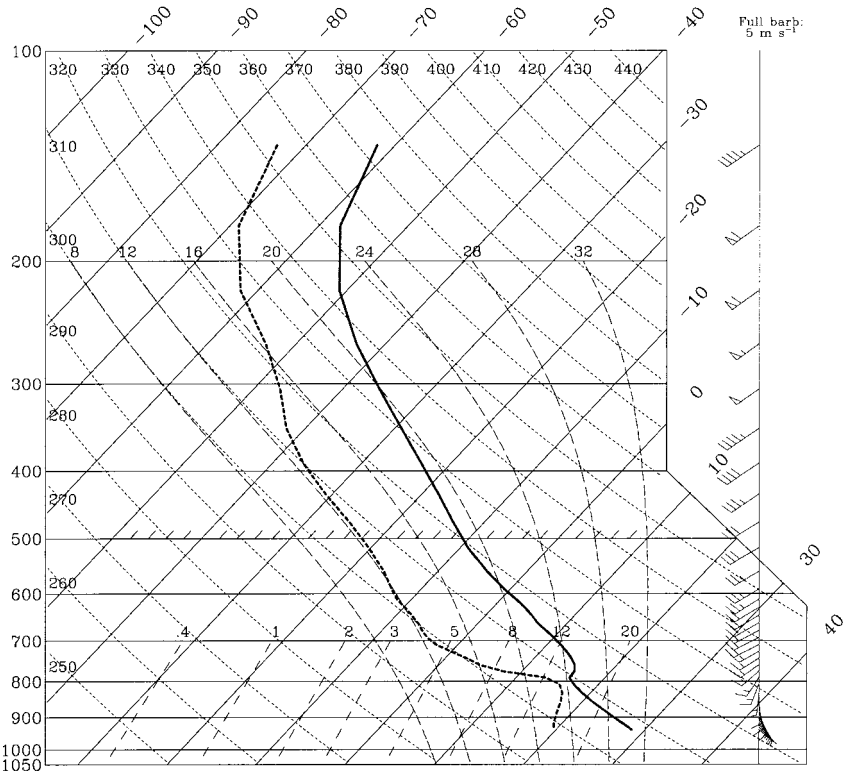

FIG. 5. The 12-h MM5 sounding near the composite MCS initiation of temperature (solid), dewpoint (dashed), and winds (flag = 25 m s^{-1}, full barb = 5 m s^{-1}).

the initiation, and the existence of an upper-level jet (to avoid repetition with Fig. 2, most of this solution is not shown).

The MM5 sounding near the time and location of the MCS initiation (Fig. 5) reveals an environment that is somewhat different from the horizontally homogenous profiles used to simulate squall lines in RKW88, WKR88, and W92. Most of the initial wind profiles in these studies have varying amounts of low-level shear, but keep the wind constant above either 2.5 or 5 km. However, in our simulation, wind speeds generally increase to a maximum near 200 hPa producing significant upper-level shear (Fig. 6 and Fig. 7c). This deep-tropospheric shear in the composite analysis reflects the tendency for warm season derecho-producing MCSs to be located near upper-level jet streams and/or jet streaks. While much of the total shear is found within the 1–3-km layer, the low-level shear vector magnitudes[2] [approximately 10.5 (15.5) m s^{-1} over the lowest 2.5 (5.0) km shown in Fig. 6] are in agreement with the results of Evans and Doswell (1998, 2001) and show little horizontal variation (Fig. 7). These magnitudes are lower than the values suggested for optimizing the strength of long-lived squall lines by RKW88, WKR88, and W92. These values are also less than the minimum low-level shear suggested by W93 for the occurrence of well-defined, long-lived bow echoes, and are at the very bottom of the range of low-level shear values that produce

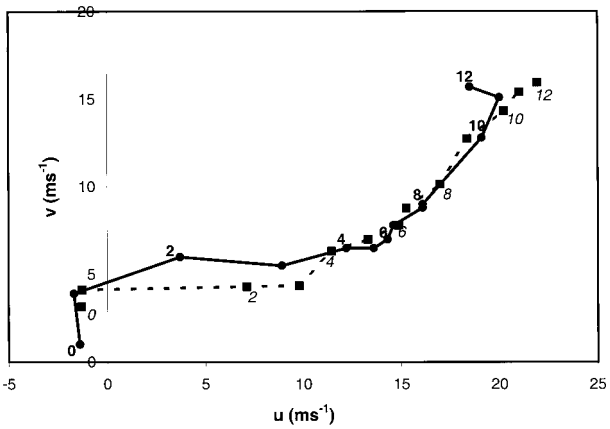

FIG. 6. Hodograph of t_o-0 composite analysis near the composite MCS initiation (solid, with bold numbers indicating the height AGL) and of the MM5 solution valid at the same time and location (dashed, with numbers in italics indicating the height AGL).

[2] It should be noted that, aside from the rotation of the wind components relative to the MCS motion, no attempt was made to preserve the vertical wind shear attributes from the individual soundings within the composite analysis. The shear values are calculated from the vector difference in the winds at each layer.

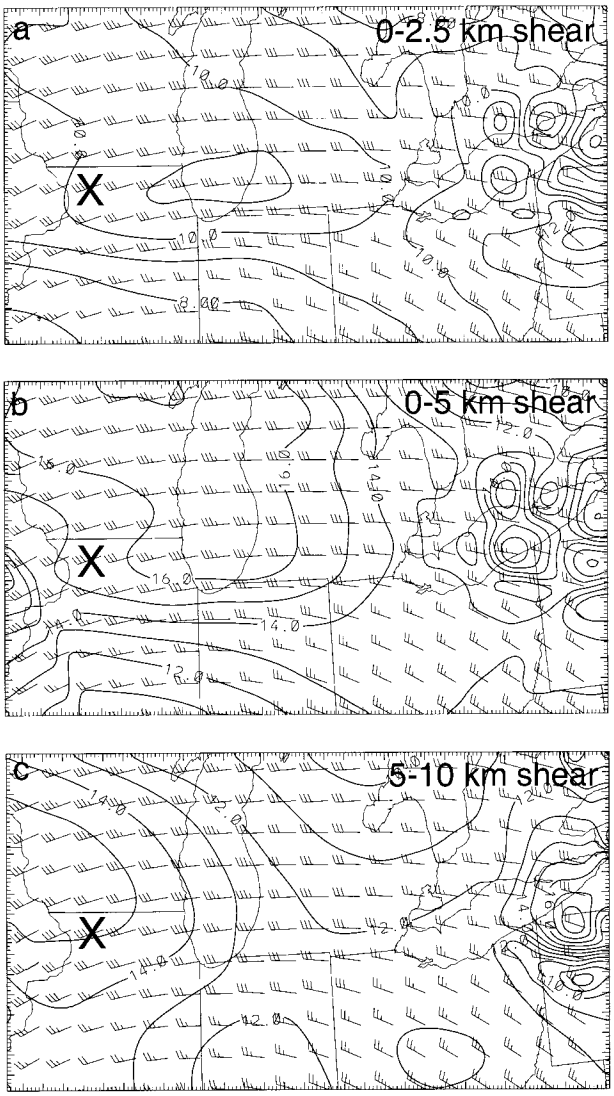

FIG. 7. Horizontal distribution of the shear at 12 h on grid 2 calculated as a vector difference of the winds between the (a) 0–2.5-, (b) 0–5-, and (c) 5–10-km levels. Vectors are plotted every eight grid points with magnitudes contoured every 1 m s^{-1}. The × denotes the location of the composite MCS initiation.

long-lived damaging wind events within the simulations presented in W93.

c. Convective initiation

The meso-α-scale warm advection and convergence in the composite analysis is enough to trigger parameterized convection on grid 1. However, the parameterization scheme does not produce saturation on the grid-scale, in the manner described by Kain and Fritsch (1998). Therefore, the usual practice of introducing warm bubbles as a convective triggering mechanism is used for this simulation (Klemp and Wilhelmson, 1978). A series of six warm bubbles with a maximum temperature perturbation, ΔT, of +4 K are introduced on grid 3 at approximately 735 min (5 min after initialization of grid 3). The centers of the thermals are approximately 35 km apart and are centered at about 1.8 km above ground level (AGL), which are similar to those used by Skamarock et al. (1994). Horizontally, ΔT decreases exponentially to zero about 15 km from the center of the perturbation. Vertically, ΔT decreases exponentially to zero about 1.8 km above and below the center of the perturbation. As stated in Skamarock et al. (1994), although this initialization is not physical, consequences of the model's response to the instantaneous heating do not appear to significantly affect the results.

Although the introduction of forcing from warm bubbles provides sufficient convergence and lift to develop individual convective cells, this convection is not able to become a self-propagating system. This is because of a small amount of convective inhibition (CIN) in the model's low-level environment (Fig. 8a). Munoz and Wilhelmson (1993) demonstrate the difficulty in sustaining grid-resolved convection that is initiated in a capped environment. However, they also demonstrate that modeled convection can move into a capped environment and sustain itself if it first develops in an environment free of CIN. Therefore, a modification to the grid-resolved specific humidity, Δq, is introduced on grid 2 prior to the introduction of the warm bubbles on grid 3 to remove a majority of the CIN and to lower the level of free convection. This modification uses a maximum Δq ($\Delta q_{\max}$) of +3.5 g kg^{-1} that is positioned at the lowest sigma level about 50 km east of the location where the warm thermals are introduced. The value of Δq decreases exponentially to zero about 150 km to the north and south, about 250 km to the east, and about 120 km west of $\Delta q_{\max}$. This same modification is introduced on each successive sigma level up to approximately 1.8 km AGL (the same sigma level at which the warm bubbles are centered). At the first sigma level above 1.8 km AGL, $\Delta q_{\max}$ is increased to +5 g kg^{-1} and decreases to zero horizontally along this sigma level in the same manner as before. However, instead of keeping this modification constant with height, this pattern decreases exponentially to zero up to approximately 3.0 km AGL. This increase in moisture above the lifting condensation level has a large influence on the ability of simulated conversion to sustain itself by reducing the entrainment of dry air and helping to preserve the positive buoyancy of the parcel (H. Brooks 2000, personal communication). Although this modification clearly alters the thermodynamic environment of the composite analysis (with a maximum CAPE increase of ~1000 m^2 s^{-2} as shown in Fig. 8b), its purpose is solely to allow the convection to become a self-propagating system. As is shown later, the convection moves out of the modified region and persists for several hours.

d. MCS simulation

Once convection persists on the inner grids, the simulation is integrated out to 24.5 h. The convection ini-

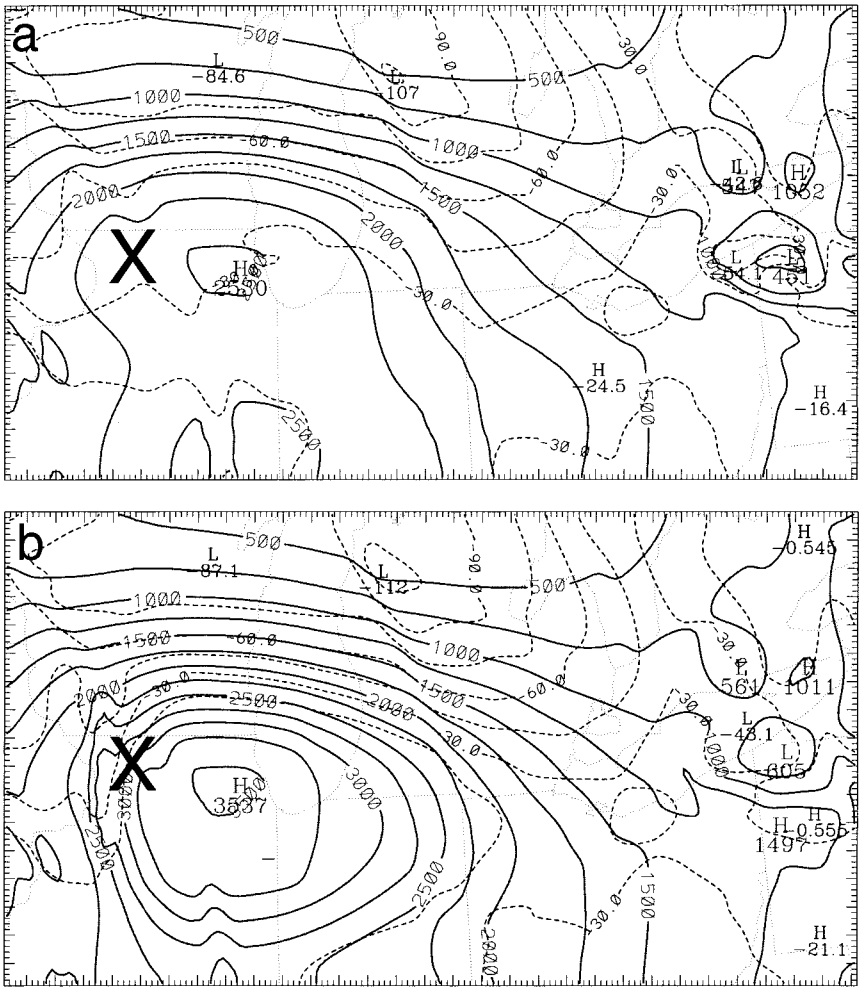

FIG. 8. (a) MM5 solution on grid 2 at the time grid 2 is initialized (12 h) of CAPE (solid, every 500 $m^2 s^{-2}$) and CIN (dashed, every 15 $m^2 s^{-2}$). (b) As in (a) except for 12.5 h (shortly after the moisture modification is introduced on grid 2). The × denotes the location of the composite MCS initiation.

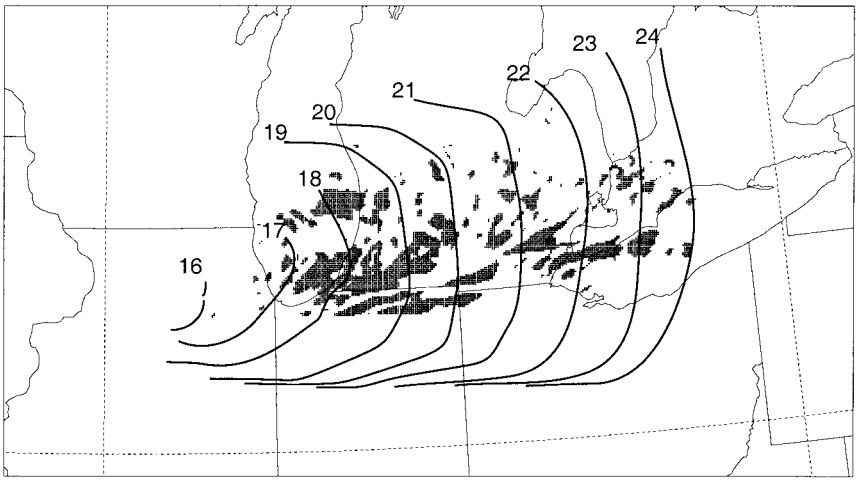

FIG. 9. Approximate hourly location of the surface gust front (solid lines) and grid points (from grid 3) with winds ≥25 m s^{-1} at the surface through 24 h (shaded regions).

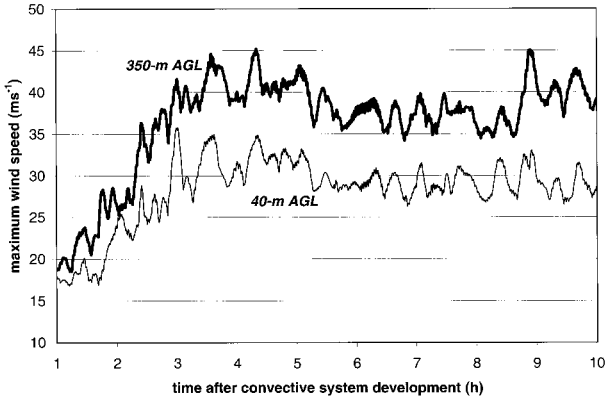

FIG. 10. Time evolution of the maximum wind speed (m s^{-1}) on the lowest grid 3 model layer (approximately 40 m AGL) and on the sigma layer at approximately 350 m AGL. A time of 4 h presented in the figure corresponds to an absolute time of 18 h in the simulation.

tiated by the warm bubbles at 12 h collapses after about 90 min. However, the explicitly resolved rainfall from each of the six cells produces several cold pools that move eastward into the modified region with little CIN (Fig. 8b). By 14 h, new cells are initiated in this region through low-level convergence and lifting along the decaying gust fronts (hereafter, the start of the MCS simulation is defined to occur at 14 h). By 16.5 h, individual, intense cells are working together to create one large cold pool. After this time, the convection organizes into a squall line–type MCS and a well-defined gust front surges to the east producing several, nearly continuous swaths of strong near-surface winds in the lowest model layer (which is approximately 40 m AGL). During this time, the main portion of the gust front is oriented almost due north–south and moves eastward at a nearly steady speed of 18–20 m s^{-1} along the quasi-stationary frontal boundary at the surface (Fig. 4). The evolution of strong near-surface winds, shown in Figs. 9 and 10, agrees spatially and temporally with many observed progressive derecho events (see Johns and Hirt 1985; Johns and Leftwich 1988; Barlow 1996; Przybylinski 1995; Bentley and Cooper 1997).

Overall, the mature system resembles a strong, asymmetric (bowing), midlatitude squall line that develops a midlevel mesoscale convective vortex (Fig. 12a) (Houze et al. 1989; Jorgensen and Smull 1993; Skamarock et al. 1994; Weisman and Davis 1998). A few embedded bow echoes develop, approximately 40–60 km in length, with enhanced system-relative rear-inflow and vorticity in mid-levels (an example is shown in Fig. 11). Isolated, intense cells develop ahead of and eventually merge with the northern periphery of the main convective line (Fig. 13); a structure found in type II progressive derechos (Przybylinski and DeCaire 1985). Other features of the mature MCS include a midlevel notch in the precipitation field at the back edge of the system (Fig. 12a), a well-defined anticyclonic outflow at upper levels above the convective core (Fig. 12b), and a region of adiabatically warmed surface air beneath the main mesoscale downdraft (not shown). These features have been frequently documented in previous observational studies of squall lines and MCSs (Goff 1976; Wakimoto 1982; Maddox 1980a, 1983; Johnson and

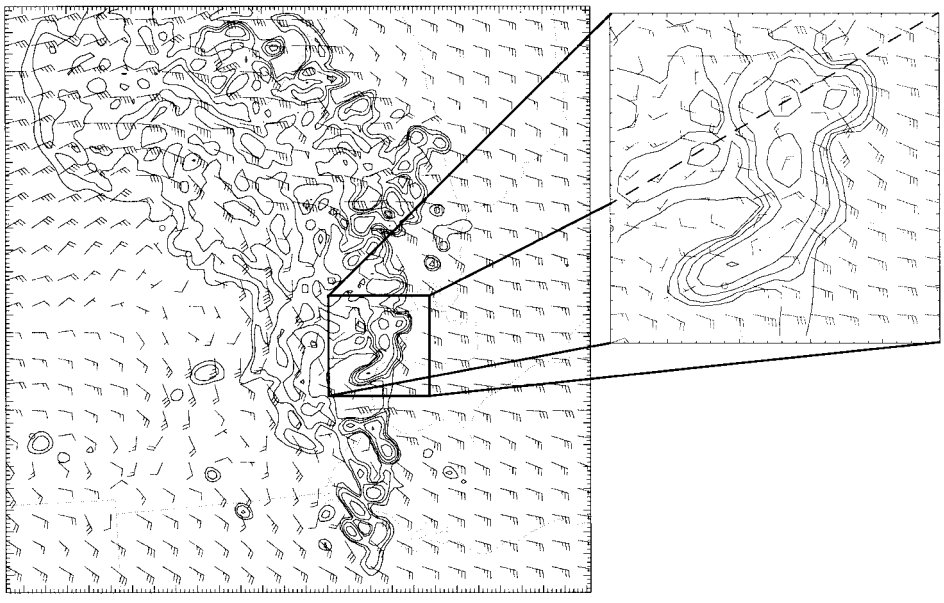

FIG. 11. The 2.5 km AGL rainwater field (contours of 0.2, 0.4, 0.8, 1.6, 3.2 g kg^{-1}) and the approximate system-relative winds (plotted every six grid points with flag = 25 m s^{-1}, full barb = 5 m s^{-1}) at 22.0 h on grid 3. Within the zoomed-in region, which has dimensions of 50 km × 50 km, winds are plotted every two grid points. Tick marks are every 2.22 km. System-relative winds are calculated by subtracting the average half-hourly velocity of the gust front from the ground-relative winds.

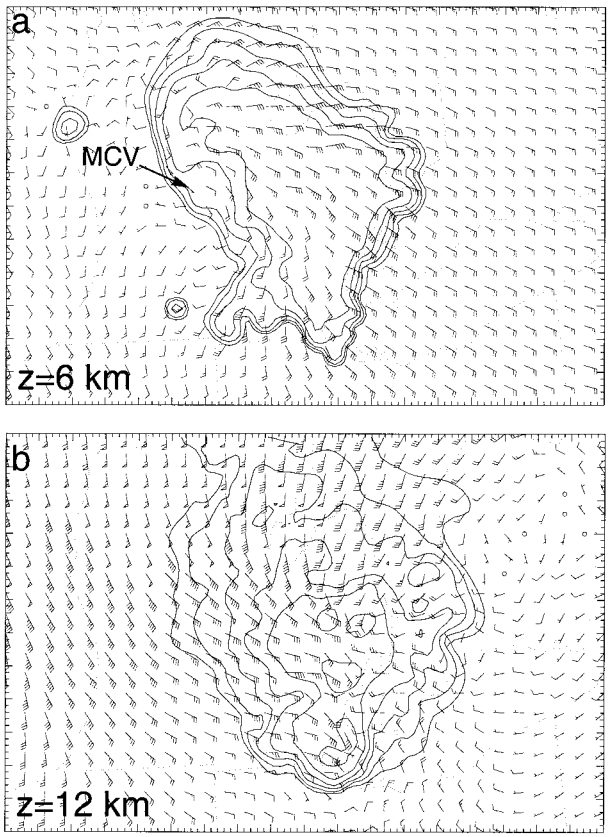

FIG. 12. As in Fig. 11 except for the total precipitation (rain and ice) mixing ratio on a 400 km × 600 km portion of grid 2 at (a) 6 and (b) 12 km.

Hamilton 1988; Houze et al. 1989; Burgess and Smull, 1990; Jorgensen and Smull 1993).

Individual convective cells are regenerated above the gust front for most of the simulation (especially along an 80–120-km portion of the leading convective line, which is shown in detail in Fig. 13), with the most intense convection occurring early in the system's lifetime in the region of maximum CAPE (Fig. 8b). The convective updrafts associated with the quasiperiodically regenerated cells along the gust front obtain an upshear tilt (Figs. 14a–c). However, these cells are quasi-steady in terms of their position relative to the leading edge of the cold pool and the tilt of the updrafts; that is, the cold pool does not surge downshear. The time-mean flow structure of these updrafts generally represents a jump and overturning updraft branch in the upper troposphere that is found within steady-state analytical models of squall lines (Moncrieff 1992). These two airflows contribute to a trailing stratiform region and a leading anvil composed of ice particles. After 21.5 h, the convective updrafts slowly become more tilted in the upshear direction (Figs. 14d,e). During this phase, rear inflow becomes well established within the cold pool resembling the structure of the idealized squall lines in W92 and the observed squall lines in Smull and Houze (1987).

In summary, this 3D numerical simulation of a progressive derecho has features that qualitatively agree with past simulations and observations. It lasts for 8 h and is still producing severe near-surface winds when the simulation is terminated, agreeing well with the average derecho lifetime of 9.2 h (JH87). The central portion of the leading convective line, where the surface outflow winds and wind shear in the inflow environment have a large component in the line-normal direction, is quasi-2D in terms of the time-mean, system-scale airflow similar to the stationary, triple-branch airflow discussed in Moncrieff (1992) and conceptualized in Thorpe et al. (1982). The time-dependent structure of the convective cells resembles the simulations of RKW88, WKR88, W92, W93, and Skamarock et al. (1994), in which the long-lived squall line is composed of individual cells that periodically generate along the gust front.

4. Comparison with past simulations

a. Local balance theory

Since the derecho simulation documented in the previous section is quasi-2D, long lived, and produces large regions of severe near-surface winds, we compare our simulation to the simulations based on local balance theory that attempt to explain squall line and bow echo strength, structure, and longevity. The conceptual model of local balance theory is explained by RKW88 and is summarized below as a convenience to the reader. The theory is quantified with the use of the 2D, Boussinesq, horizontal vorticity equation in flux form (neglecting friction):

$$\frac{\partial \eta}{\partial t} = -\frac{\partial (u\eta)}{\partial x} - \frac{\partial (w\eta)}{\partial z} - \frac{\partial B}{\partial x}, \tag{1}$$

where $\eta = (\partial u/\partial z - \partial w/\partial x)$ is the line-normal component of horizontal vorticity and

$$B \equiv g\left(\frac{\theta'}{\bar{\theta}} + 0.61q_v' - q_c - q_r\right) \tag{2}$$

is the buoyancy with potential temperature, θ; water vapor mixing ratio, q_v; cloud water mixing ratio, q_c; and rainwater mixing ratio, q_r (primes denote deviations from the mean state, which is given by the overbar symbol). By fixing the frame of reference to follow the gust front, (1) can be integrated within an area that encompasses the leading edge of the cold pool to obtain

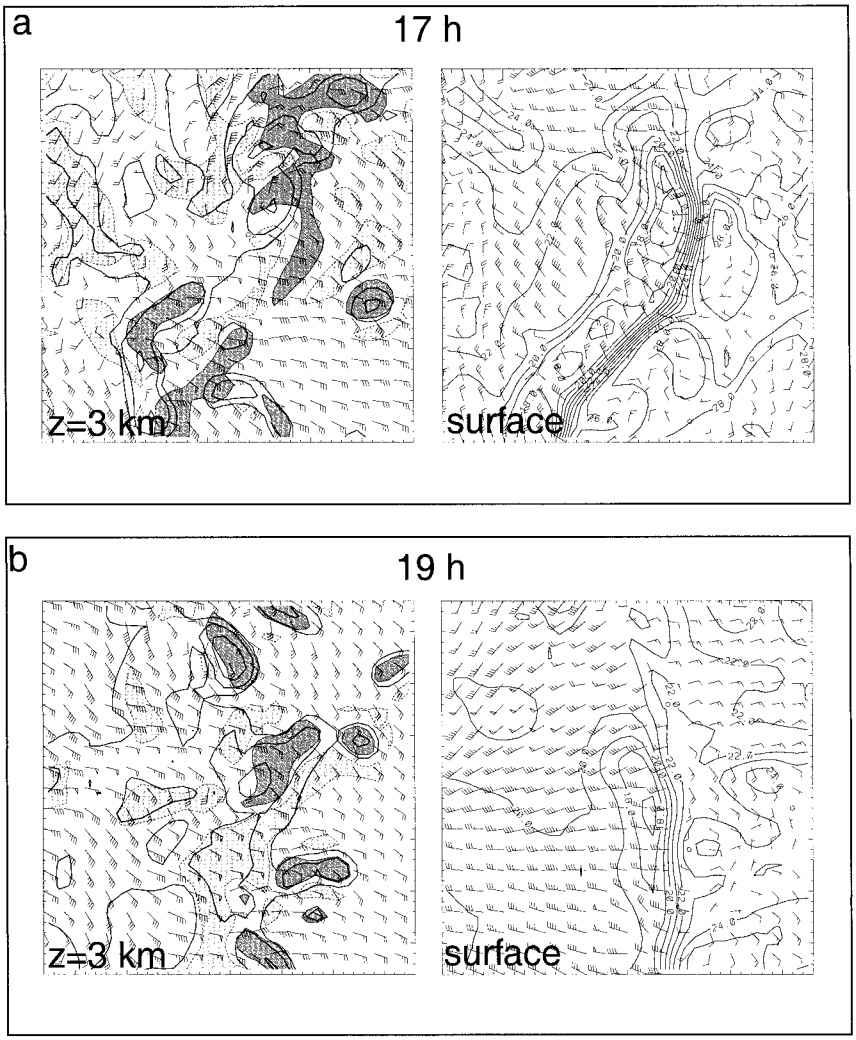

FIG. 13. Conditions at 3 km and at the surface for an 80 km × 80 km region along the leading edge of the simulated convective system at (a) 17, (b) 19, (c) 21, and (d) 23 h. The 3-km plots display the rainwater mixing ratio (solid contours of 0.2, 0.4, 0.8, 1.6, 3.2, g kg^{-1}), vertical velocity $\geq$3 m s^{-1} (darkly shaded regions enclosed with thin contours), vertical velocity ≤ -1.5 m s^{-1} (lightly shaded regions enclosed with thin dashed contours), and system-relative winds as in Fig. 11. The surface plots display temperature (solid contours every 1°C) and ground-relative winds (flag = 25 m s^{-1}, full barb = 5 m s^{-1}).

$$\underbrace{\frac{\partial}{\partial t}\int_L^R \int_0^d \eta \, dz \, dx}_{\text{I}} = \underbrace{\int_0^d (u\eta)_L \, dz}_{\text{II}} - \underbrace{\int_0^d (u\eta)_R \, dz}_{\text{III}} - \underbrace{\int_L^R (w\eta)_d \, dx}_{\text{IV}} + \underbrace{\int_0^d (B_L - B_R) \, dz}_{\text{V}}, \quad (3)$$

where L and R represent the left (upshear) and right (downshear) edges of the area, respectively, and 0 and d represent the ground and the top of the area, respectively. In this framework, the gust front propagates in the downshear direction. Terms II and III in (3) represent the horizontal vorticity flux through the area, term IV represents the vertical flux of vorticity out the top of the area (it is assumed that $w = 0$ at the surface), and term V represents the net generation of vorticity from horizontal buoyancy gradients. The total tendency term (term I) is set to zero to solve for the possible steady-state solutions. RKW88 assume that the ambient buoyancy (B_R) is negligible and that $\eta \cong (\partial u/\partial z)$ near the left and right edges of the area. Furthermore, $u_{L,0}$ is set to zero to describe stagnant flow inside the cold pool. They also assume no relative flow above the height of the cold pool top, H (where $H \leq d$), so that $u_{R,d} = u_{L,d}$

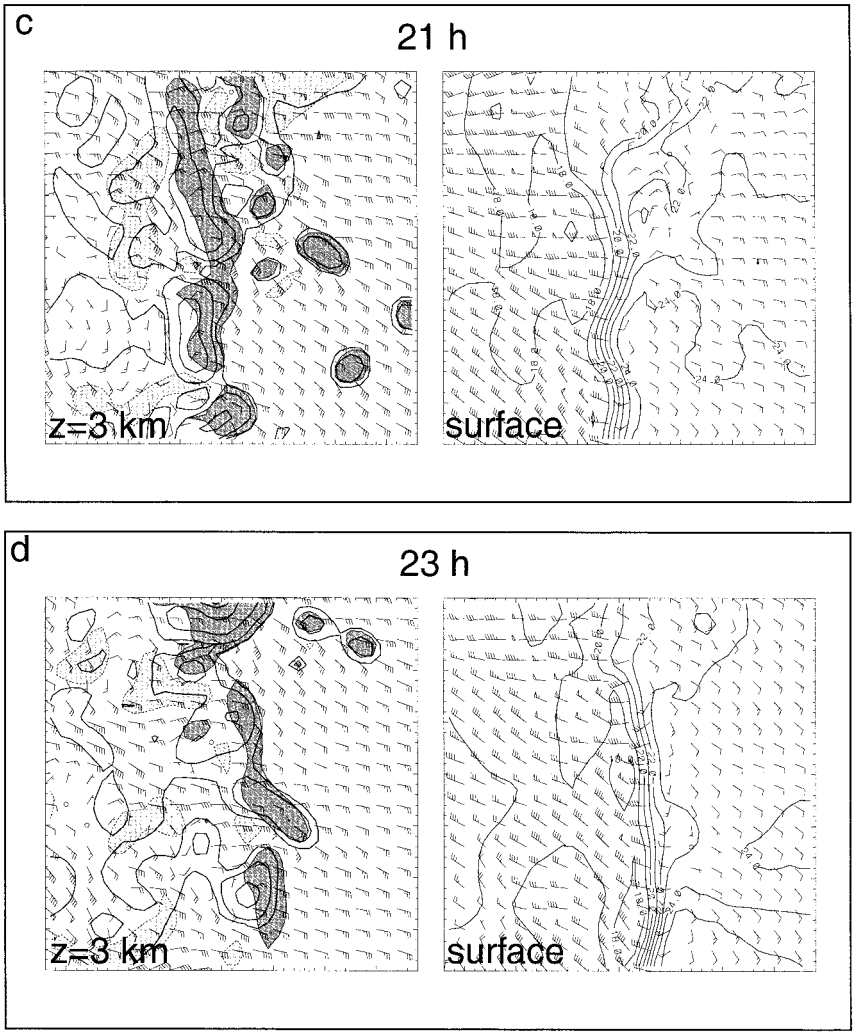

FIG. 13. (*Continued*)

$= 0$. In conjunction with this assumption, the authors impose a solution whereby the updraft is symmetric and vertically erect at the leading edge of the cold pool. This situation should then produce the deepest lifting at the leading edge of the cold pool if local vorticity balance is a primary factor. Therefore, they set

$$\int_L^R (w\eta)_d \, dx = 0 \tag{4}$$

in (3). Under these assumptions, (3) reduces to

$$\Delta u^2 \equiv (u_{R,0}^2 - u_{R,d}^2) = 2 \int_0^H (-B_L) \, dz \equiv C^2, \tag{5}$$

which can be conveniently expressed by the ratio

$$\frac{C}{\Delta u} = 1, \tag{6}$$

which is the optimal solution of local balance theory. The physical interpretation of (6) is that the import of the positive vorticity associated with the low-level shear just balances the net buoyant generation of negative vorticity by the cold pool in the volume. Under this optimal state ($C = \Delta u$), the simulated squall lines approximate a steady state through the nearly continuous development of nearly erect updrafts directly along the gust front. Under the less than optimal state ($C > \Delta u$), the simulated squall lines become progressively weaker with time in response to the strengthening cold pool circulation.

Within the squall line simulations of W92, upshear-tilted updrafts that develop during the less than optimal state create horizontal buoyancy gradients along the back edge of the system, which generates circulations leading to the development of rear inflow. The local balance theory described above is modified by W92 in an attempt to explain how this relative flow within the cold pool may act to reestablish an optimal state along the gust front. By retaining the term $\Delta u_j^2 \equiv (u_{L,H}^2 -$

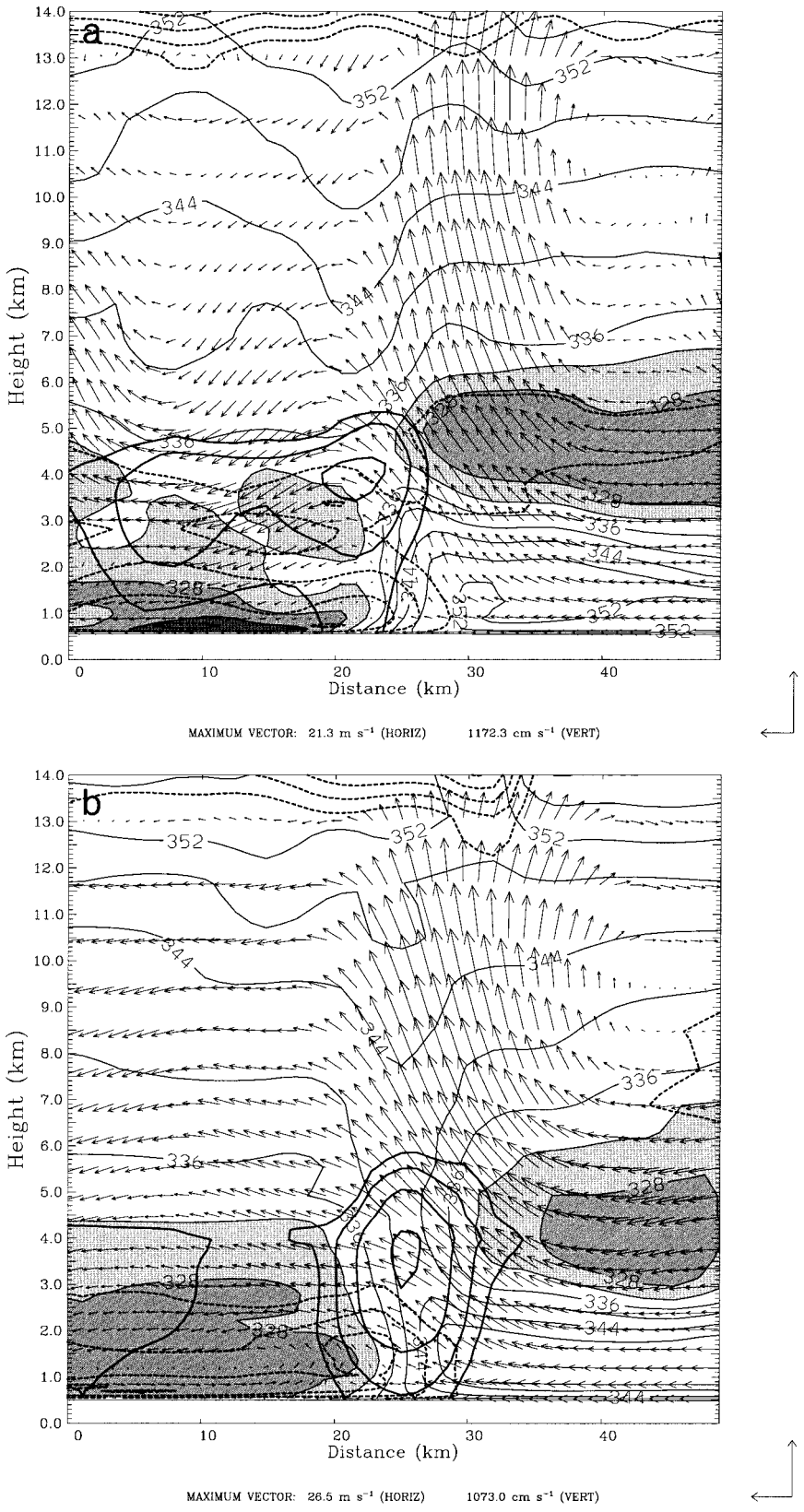

FIG. 14. The E–W line-averaged vertical cross sections along the leading edge of the convective system (values are averaged through a total of 25 km in the meridional direction). Displayed is the rainwater mixing ratio (thick solid lines contours of 0.5, 1.0, 2.0, 4.0 g kg^{-1}), equivalent potential temperature (thin solid lines contoured every 4 K with values less than 332 K shaded), negative values of perturbation

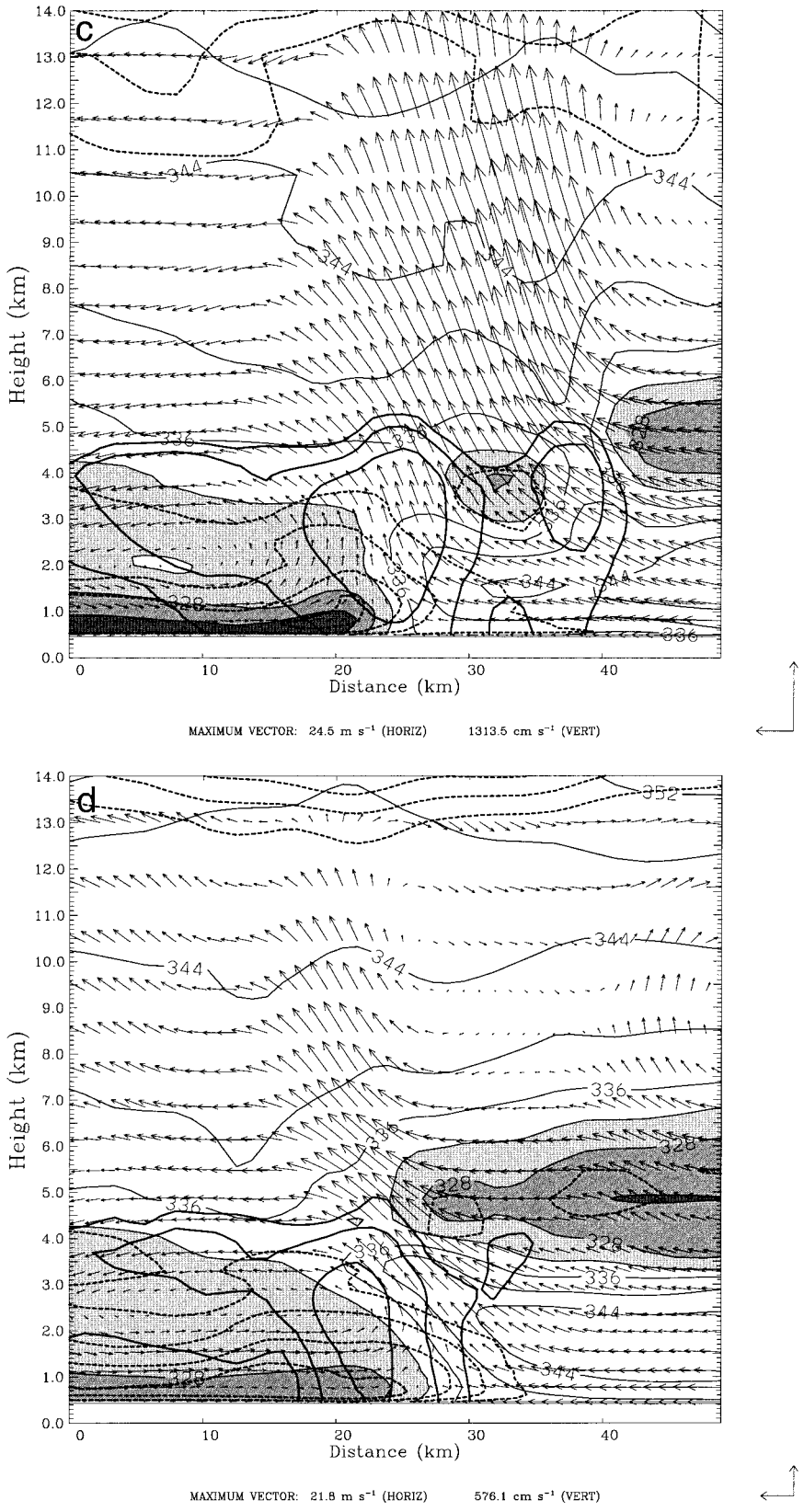

FIG. 14. (*Continued*) temperature (thin dashed lines every 2 K with the zero line omitted), and the system-relative winds (m s^{-1}) at (a) 16.5, (b) 18.5, (c) 20.5, (d) 22.5, and (e) 24.5 h. The maximum horizontal and vertical wind vector is defined below each plot.

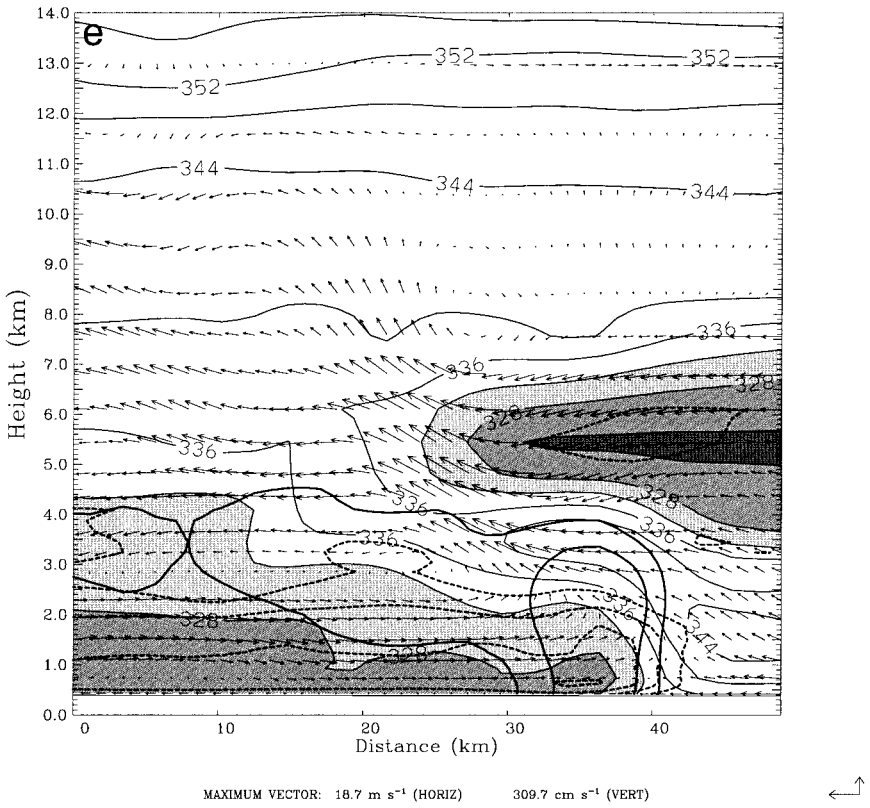

FIG. 14. (*Continued*)

$u_{L,0}^2$) in the integration of (3), which represents shear within the cold pool itself, W92 shows that the balance condition of (5) becomes

$$\Delta u^2 = C^2 - \Delta u_j^2 \equiv C_j^2. \tag{7}$$

Calculations of (7) for a particular simulation in W92 illustrate that a value of $C_j/\Delta u = 1$ can represent a steady, optimal state for the maintenance of squall lines that contain strong, elevated rear-inflow jets. Physically, the positive vorticity associated with an elevated rear-inflow jet counteracts the negative vorticity generation by the cold pool, which reverses the weakening process and helps to bring the squall line back to an optimal state. W92 also shows that values of $C_j/\Delta u > 1$ can support a system that becomes progressively weaker and more upshear tilted with time, with rear inflow that descends to the surface well behind the main convective line. In this case, the rear inflow enhances the effects of the cold pool circulation and hastens the weakening process. In general, squall lines with significant, elevated, system-relative rear inflow jets require at least 15 m s^{-1} of shear in the lowest to 2.5 km within the simulations of W92. Within the simulations of W92, in which the shear is distributed over the lowest 5 km, squall lines with strong, elevated rear inflow become restricted to environments with larger shear and larger CAPE than for the shallow-shear simulations.

b. Comparison to previous idealized simulations

Since local balance theory is developed in a 2D framework, calculations[3] of (6) and (7) are performed along several portions of the simulated system that qualitatively resemble a 2D steady convective system, in which the flow has a large component in the line-normal direction. For each calculation, the ambient shear is calculated using average variables within a 10 km × 20 km area approximately 100 km downshear of the gust front to ensure that the solutions are not contaminated by convection. The parameters relevant to the cold pool (C and Δu_j) are calculated using average variables within a 10 km × 20 km area centered approximately 15 km behind the gust front, which is similarly done in W92. The base-state potential temperature, contained in the definition of B in (2), is defined to be a 2D north–south cross section approximately 100 km east of the convective system. The height of the cold pool top, H, is defined using a value of buoyancy (B_{top}). From an examination of the gust front speed and the buoyancy distribution, it is found that the motion of the cold pool is largely described by density current dynamics (Ben-

[3] The development of the theory allows an arbitrary height, $d \geq H$, to be used in the shear calculations. However, as done in W92, it is convenient to let $d = H$ for the present simulation.

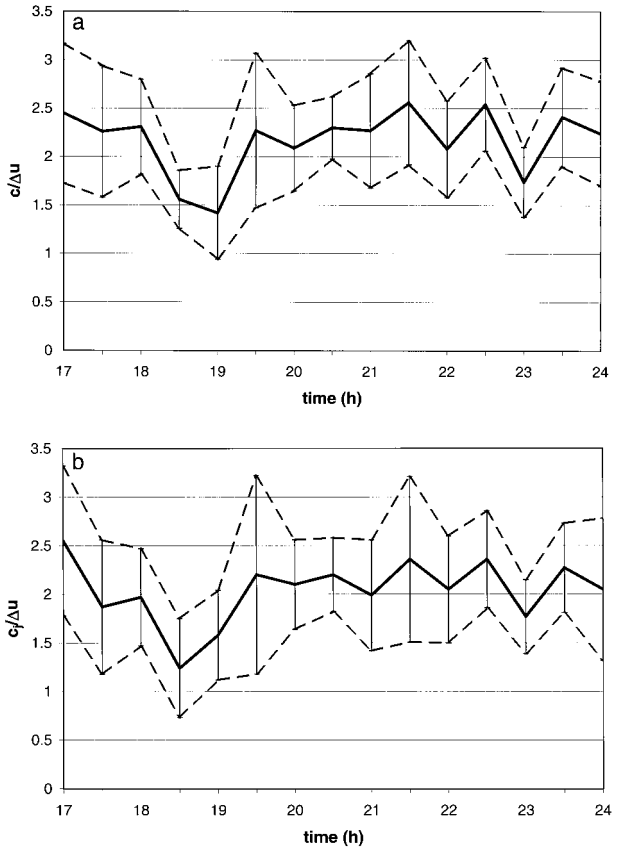

FIG. 15. An example of the time evolution of the balance conditions (solid lines) given by (a) Eq. (6) and (b) Eq. (7) along a central portion of the gust front. The short dashed lines denote plus/minus one standard deviation calculated within the 10 km × 20 km area used to make the calculations.

jamin 1968; Simpson and Britter 1980). Using the relationship for the speed of atmospheric density currents given by Seitter (1986) as an estimate, it is found that a value of $B_{\text{top}} = -0.06$ m s^{-2}, which corresponds to a potential temperature perturbation of about -2 K, gives a good approximation to the true gust front speed. Using this value of B_{top}, H generally remains steady between 2 and 3 km AGL throughout the simulation.

For this simulation, calculations using (6) and (7) indicate that the environment in which the derecho-producing MCS develops is significantly less than optimal and remains so through the end of the simulation, even when accounting for the relative flow within the cold pool (an example of one such calculation is shown in Fig. 15). It should be noted that the values of $C/\Delta u$ and $C_j/\Delta u$ show little sensitivity to the chosen value of B_{top} and the chosen location for the calculations along the squall line leading edge (not shown). Therefore, Fig. 15 approximates the local balance conditions of the system as a whole. RKW88 find that once these conditions are met within their simulated squall lines, ''even when the low-level air is lifted above its level of free convection, and above the shear zone at the top of the cold outflow, no new vigorous cells are triggered'' (p. 477 of RKW88). Within this particular simulation of RKW88, 90 min after the squall line enters the less than optimal state, the greatest concentration of rainwater is found approximately 40 km behind the gust front as the cold pool surges downshear. They conclude that under these conditions, the circulation progressively leans farther upshear as the cold pool dominates the circulation and that only a matching positive vortex associated with the low-level shear can maintain the updrafts above the gust front. Similarly, WKR88 present a simulation initialized with 10 m s^{-1} of shear over the lowest 2.5 km, which fails to produce significant rainfall beyond 3 h. Within this simulation of WKR88, the regenerated cells become much weaker with time and are centered 50 km behind the gust front by 4 h. In addition, the 3-km system-relative flow remains front to rear at all times, and the front-to-rear flow above the cold pool rapidly develops (see Fig. 10a of WKR88). The decaying phases of these squall lines are seen to be directly related to an imbalance between the cold pool and the low-level shear. Again, these particular simulations presented in RKW88 and WKR88 have constant winds above 2.5 km.

In the present simulation, which has shear throughout the depth of the troposphere, but a similar 0–2.5-km shear vector magnitude (10–11 m s^{-1}) and a similar less than optimal balance condition from the start of the simulation, the system contains *persistent,* convective updrafts that retain a nearly constant tilt with the convective cores remaining above the cold pool leading edge (Fig. 14a-c). Thus, while the updrafts have an upshear tilt, the gust front does not surge out ahead of the updrafts as it does in the simulations presented in RKW88 and WKR88 with similar 0–2.5-km shear and balance conditions (see Fig. 12 of RKW88 and Fig. 4 of WKR88). The same conclusion can be made when comparing our simulation within the simulation of W92 with similar low-level shear and balance conditions (see his ''moderate shear'' simulation). The fact that intense cells are generated by the gust front under much less than optimal conditions does not necessarily, in itself, present a disparity with the expectations of local balance theory since we do not know how the intensity and tilt of the updrafts would change with varying low-level shears. However, within the idealized simulations reported in RKW88 and WKR88, updrafts that *maintain* their relative tilt and remain aligned with the gust front for more than 3 h only occur for the stronger shear simulations, in which the environment provides close to or greater than optimal balance conditions. Rotunno et al. (1990) argues that an appropriate balance between the low-level shear and the cold pool is ''a necessary (clearly not a sufficient) requirement for sustaining most strong squall lines'' (p. 1033); a statement that is not supported by this realistic model simulation.

Examination of Figs. 13 and 14 reveals that our simulation has more resemblance to the simulations with stronger low-level shear presented in WKR88 and W93.

In particular, notice the intense cell at 17 h (Fig. 13a) with a well-defined cyclonic vortex at 3 km AGL. As can be seen in Fig. 9 and Fig. 13, this cell evolves into a bow echo and produces a long swath of severe near-surface winds. Even 8 h after the system develops (22 h), the system contains a bow echo (Fig. 11) with a significant cyclonic vortex along its northern end and moderate rear inflow at 2.5 km. Even at this later time, the majority of the main, convective elements continue to be located close to the leading edge of the cold pool (Fig. 13d). This shows that the system clearly does not resemble the ''weak'' squall line system described in W93, in which cells are found tens of kilometers behind the gust front within a few hours after the system develops (see his Fig. 23). Within the simulations of W93, these weak squall lines develop for all cases with 15 m s^{-1} of shear or less over the lowest 2.5 or 5 km, independent of the amount of CAPE in the environment (see his section 6a).

The evolution of the maximum near-surface winds suggests that the system is not weakening over time with values that remain at or above severe limits for the entire simulation period (Fig. 10). When compared with the simulations of W93 with similar CAPE and low-level shears (see his Fig. 25), one could argue that our simulation produces stronger 350-m wind speeds. However, we recognize that one of the difficulties in defining squall line strength is choosing an appropriate metric (WKR88 use total condensate, W92 uses maximum rear-inflow strength, and W93 uses the near-surface winds). If we use 350-m winds as a measure of squall line strength, then our simulation appears to be as strong as any of the simulations reported in W93, even for low-level shears twice as large as those found in our simulation. Therefore, because of the inaccuracies involved, it is likely that no single metric, including the near-surface wind, is fully able to quantify squall line strength and that perhaps it is more reasonable to examine updraft evolution as a means to compare the behavior between the simulations.

As stated in RKW88, the optimal state contains updrafts that maximize their full CAPE potential (correcting for dilution and water loading). In a time series of maximum vertical velocity (w_{MAX}), these optimal updrafts display oscillatory behavior with large-amplitude variations about a steady value (see Fig. 10 and Fig. 13 of RKW88).

Conversely, the less than optimal state contains updrafts that are only minor perturbations on the general circulation and are fundamentally different from the large-amplitude cells of the optimal state. These updrafts have their energy progressively depleted by the increasingly dominant circulation of the cold pool. This implies that even within an environment in which the background CAPE does not vary, a cold pool that causes convection to lean upshear leads to less-vigorous further convection with smaller values of upward motion relative to their CAPE potential.

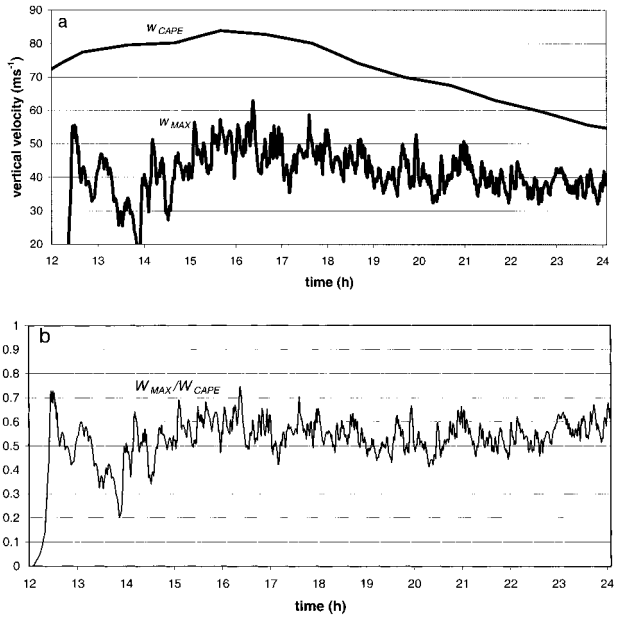

FIG. 16. (a) The maximum vertical velocity (w_{MAX}) from the simulation and the estimated maximum vertical velocity from Eq. (8) (w_{CAPE}). The ratio of these quantities is shown in (b).

To more clearly examine the behavior of the cells from our simulation in this regard, we compare w_{MAX} to the expected maximum vertical velocity (w_{CAPE}) from the relationship

$$W_{CAPE} = \sqrt{2 \times CAPE}, \tag{8}$$

where the CAPE is calculated using the cloudy virtual temperature correction given in Carpenter et al. (1998). Using this relationship, we can examine whether or not the cells are weakening relative to their potential by filtering out the decreases in w_{MAX} due to the decrease in CAPE along the path of the derecho. As the system progresses eastward, the convective system moves into an environment with increasingly less CAPE (approximately 1000 m^2 s^{-2}) and a higher level of free convection by 24.5 h (Fig. 8b). Without correcting for dilution and any model inaccuracies, w_{CAPE} overestimates the updraft strength at all times, as expected (Fig. 16a). By examining the updrafts, *in relation to the CAPE in the environment* (w_{MAX}/w_{CAPE}), the magnitudes of the updrafts are not becoming significantly weaker with time relative to their maximum potential (Fig. 16b). The evolution of the near-surface winds (Fig. 10), which clearly are not weakening with time, is consistent with this result. While the inability to precisely determine the effects of dilution limits the quantitative assessment of these results, this suggests that the cold pool is not depleting the newly triggered cells of their energy as it does in the weakening (less than optimal) phase of the RKW88 simulations. This indicates that the lessening of the *absolute* strength of the updrafts may be controlled more by the decrease in CAPE along the system's

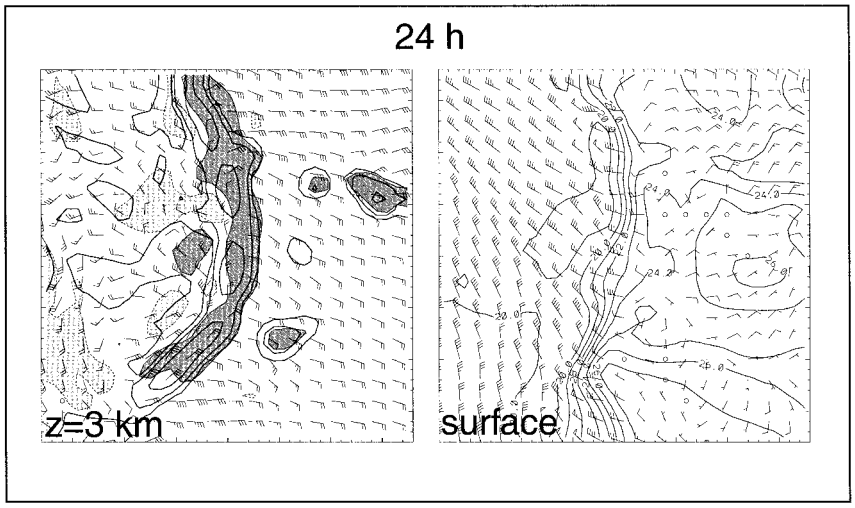

FIG. 17. The 3 km AGL and surface conditions at 24 h, as in Fig. 13, for the sensitivity run with increased CAPE along the system's track.

track rather than a local vorticity imbalance along the system's leading edge.

This hypothesis is tested by modifying the low-level moisture in the MM5 initial condition in order to produce larger CAPE values to the east of the region of convective development. Thus, instead of the CAPE decreasing from 3500 to 1000 $m^2\ s^{-2}$ (see Fig. 8b), the CAPE decreases from 3500 to only about 2200 $m^2\ s^{-2}$ over the lifetime of the convective system. Results from a simulation using this modified initial condition show that the convective line at 24 h continues to produce much stronger and more vertically oriented updrafts (Fig. 17), some of which continue to evolve into bow echoes (Fig. 18), even though a less than optimal balance condition is maintained throughout the simulation. These results further suggest that the decreasing trend in the mean w_{MAX} seen after 16.5 h is more strongly related to the decrease in CAPE along the system's track, rather than a local vorticity imbalance. This conclusion is also supported by the results of Garner and Thorpe (1992, hereafter GT92), who suggest that the strength and structure of their simulated squall lines are more related to the potential buoyant energy within the inflow layer than the direct interaction of the cold pool with the low-level environmental shear.

To summarize, the evolution of quasiperiodically generated updrafts directly above the gust front to highly slanted and much weaker updrafts (in an absolute framework) is similar to the evolution of the simulated squall lines presented in RKW88 and WKR88. However, the fundamental difference between the present simulation and these previous, idealized simulations is the timescale at which this evolution occurs. For a simulation initiated with 10 $m\ s^{-1}$ of shear over the lowest 2.5 km and no shear above this level, RKW88 find that there is only one full oscillation of the large-amplitude updrafts covering a time span of about 90 min before the line enters its weaker mode. The primary mechanism by which the squall line weakens is the increasing dominance of the cold pool circulation, which leads to less vigorous further convection and more of a mean, upshear tilt with time. In our simulation, which has shear throughout the depth of the troposphere but a similar 0–2.5-km shear vector magnitude of 10–11 $m\ s^{-1}$, the updrafts do not lean more upshear with time until at least 6 h after the system develops, even though the cold pool dominates the low-level shear from the start of the simulation. In addition, during this upshear tilting phase, the updrafts do not appear to be weakening relative to their CAPE potential, which contradicts the updraft behavior in the less than optimal state of the RKW88 and WKR88 simulations. These same inconsistencies in updraft evolution are also found when comparing our simulation with the simulations presented in WKR88, W92, and W93 for relatively weak shears over the lowest 5 km. Since the simulated squall line produces severe, near-surface winds for over 8 h; contains convective updrafts that remain directly above the gust front; and has both storm-scale and MCS-scale features of many observed progressive derechos, the local balance theory appears incomplete as it applies to the present simulation. The reason why the strong cold pool does not surge downshear and continues to produce *and sustain* intense convection for a several hour period needs to be understood.

c. Another environmental factor to consider

The previous section indicates that our simulation evolves in a manner somewhat inconsistent with previous, idealized simulations of squall lines within a similar low-level kinematic environment. The main difference is the persistent, quasiperiodic development of cells *directly above the gust front* with a *quasi-steady*

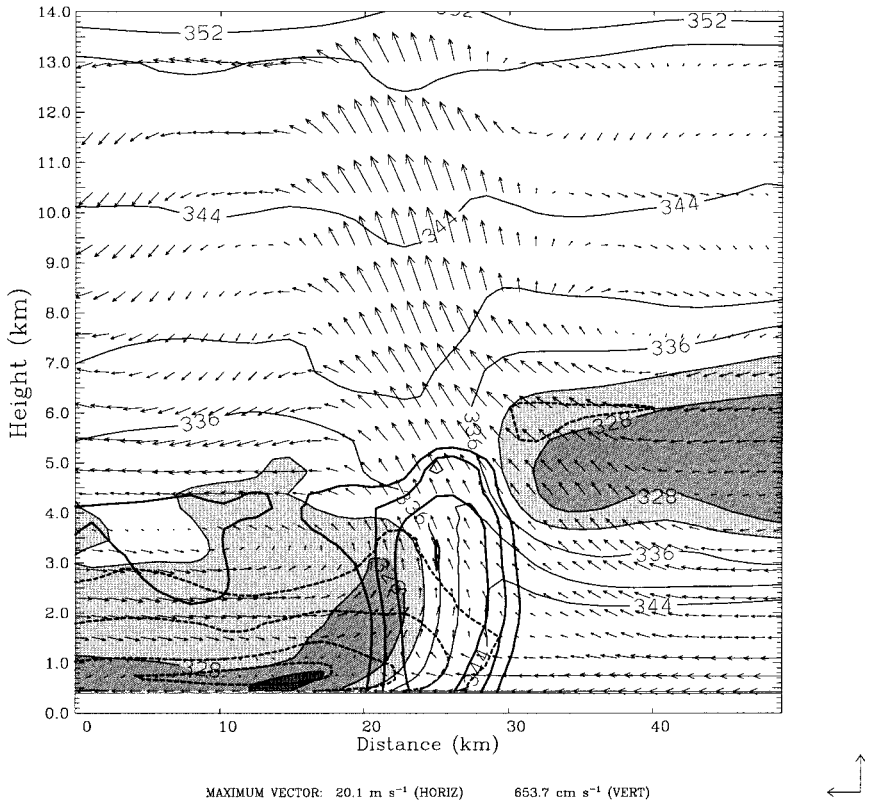

FIG. 18. Vertical cross-section at 24 h, as in Fig. 14, for the sensitivity run with increased CAPE along the system's track.

upshear tilt despite a much less than optimal condition of local balance theory. A possible explanation for this may arise from the existence of strong, upper-tropospheric winds and the associated shear throughout the depth of the troposphere in the preconvective environment (Figs. 5–7), which has not been considered in the development of the local balance theory. Many particularly severe progressive derecho events documented in the literature also display a wind profile in the preconvective environment with significant unidirectional mid- to upper-level shear (see Johns and Hirt 1985; Schmidt and Cotton 1989; Przybylinski 1995; Barlow 1996; Bentley and Cooper 1997). It appears that a more complete dynamical explanation for severe, long-lived squall lines, in regards to the convective response to the shear, should include the possibility of variations in relative flow in the upper troposphere in relation to the movement of the gust front.

One theory that includes the influences of deep-tropospheric wind shear is the global dynamics theory as discussed in Lafore and Moncrieff (1989, 1990) and GT92. These studies suggest that local vorticity balance along the outflow leading edge is secondary in importance to the larger circulations around the squall line in modulating the intensity of the convection and that the shear throughout the depth of the troposphere must be considered. Similar to the results of RKW88, GT92 shows that a minimum threshold *total* shear (the product of the shear magnitude and the depth of the shear layer) is needed to support strong, quasi-steady squall lines in their idealized simulations. Within local balance theory, RKW88 states that ''since cold pools are located at low levels, the shear can promote convection only when restricted to low levels'' and that ''it is the actual shear within the air that makes contact with the cold pool that is influential, not simply the velocity difference between the subcloud and cloud-bearing layer'' (p. 477). However, for one particular simulation presented in GT92 (see p. 113 of GT92) initiated with an elevated shear layer, and no ambient shear throughout the depth of the cold pool, a quasi-steady squall line still develops with a flow structure similar to the 2D analytical framework. In this case, the height of the shear layer eliminates any *direct,* physical interaction between the ambient vorticity and that generated by the cold pool. In terms of the relevant physics, initial environments with deep-tropospheric shear, which contain a steering level, and large CAPE can facilitate a deep, overturning circulation upstream from the gust front, regardless of the low-level shear. Under these circumstances, deep-tropospheric shear allows the initial subsidence to occur ahead of the gust front and aids in the development of an upper-level overturning branch, which subsequently helps to maintain the convection close to the gust front leading edge.

This implies that increases in potential buoyancy within the inflow layer make it easier for the shear to align the convective updrafts with the gust front.

Although unable to explicitly determine the effects of *low-level* shear, Shapiro (1992) shows that, despite relatively weak mean ascent along a density current barrier, an environment with deep-tropospheric shear increases the residence time of air parcels within the region of upward motion creating a much greater likelihood of initiating and/or maintaining deep convection. Similarly, Moncrieff and Liu (1999) show that downshear propagating cold pools within deep-tropospheric shear provide the deepest lifting if they move at the speed of the ambient flow at a critical (steering) level.

In a series of analytical and numerical experiments of density currents that includes variable upper-level shear, Xue (2000) finds that deep-tropospheric shear can be as important as the low-level shear in determining the uprightness of the upward branch of inflow. Xue further suggests that the difference in the flow speeds between the subcloud and cloud-bearing layers may be more important than the presence of positive shear in the lowest levels for sustaining deep convection along the density current.

While the ideas emphasizing the importance of deep-tropospheric shear present an intriguing alternative, most of these simulations are constrained by the initial specifications of the flow field and characteristics of the convection, unlike the numerical simulations upon which the local balance ideas are based. Therefore, to examine the importance of upper-level shear to squall line strength and longevity in this modeling capacity, we use a 2D version of the Collaborative Model for Mesoscale Atmospheric Simulation (COMMAS; Wicker and Wilhelmson 1995), which is very similar to the model (Klemp and Wilhelmson 1978) used by RKW88, WKR88, and W93. The model initial conditions are horizontally homogeneous over a 380 km $\times$ 17.5 km grid domain with 1.0-km horizontal and 0.5-km vertical grid spacing. The model initial conditions are horizontally homogeneous and use the same thermodynamic sounding as RKW88 and WKR88.

These additional simulations highlight behaviors similar to those found when comparing our MM5 simulation to the RKW88 and WKR88 simulations. The experiments with shear only over 0–2.5 km agrees with RKW88 and WKR88 in that the stronger low-level shear cases produce stronger updrafts and the maximum updraft strength becomes smaller in magnitude with time and contains much smaller variations in amplitude once the cold pool dominates the circulation after a few hours (Fig. 19, dark lines). These results are altered, however, when shear is added above 5 km. For the weak shear case (10 m s^{-1} shear over 0–2.5 km), when additional wind shear is added above 5 km (10 m s^{-1} shear per 5 km above 5 km, very similar to the upper-level shear in the MM5 simulation), the strength of the simulated squall line is maintained over a much longer period (Fig. 19a). For the stronger shear case (17.5 m s^{-1} of shear over 0–2.5 km), when the same additional wind shear is added above 5 km the simulated squall line has more intense updrafts after 3 h (Fig. 19b). While the maxi-

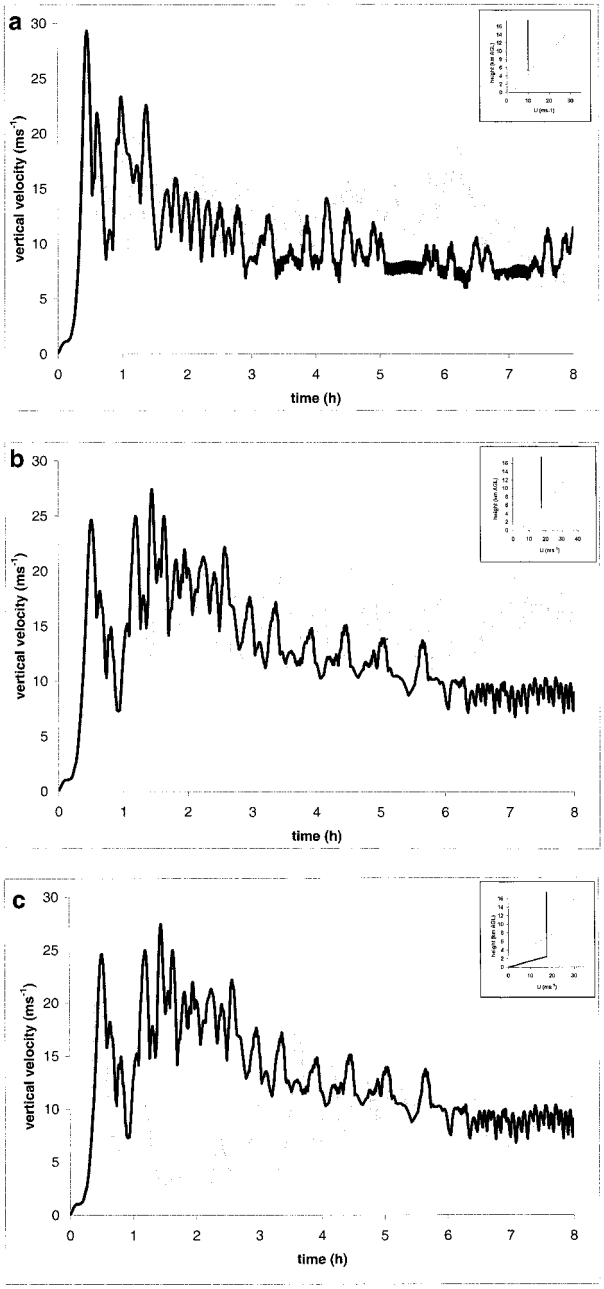

FIG. 19. Maximum vertical velocity (m s^{-1}) vs time (h) in the two-dimensional model domain for the (a) 10 m s^{-1} weak low-level shear case and (b) 17.5 m s^{-1} stronger low-level shear case. Dark lines are from the runs in which the shear is restricted to the lowest 2.5 km using the shear values mentioned. Light lines are from the runs with the same shear below 2.5 km, but with an additional 10 m s^{-1} of shear per 5 km above 5 km. (c) A comparison of the 17.5 m s^{-1} low-level shear case (dark line) with a simulation with no shear in the lowest 2.5 km and 10 m s^{-1} of shear per 5 km between 2.5 and 10 km (light line).

mum updraft strength is somewhat weaker during the first 3 h when mid- to upper-level shear is added (Figs. 19a,b), it is much more difficult to define when the squall lines enter a weaker state both in terms of the absolute magnitude of the updrafts and the amplitude of the updraft oscillations. For the second case in particular (Fig. 19b), the simulation with mid- to upper-level shear appears to enter a quasi-steady state at the same time the simulations with only low-level shear appear to enter their weaker phase (at about 2.5 h). This shows that the addition of upper-level shear can maintain the strength of simulated convective lines over much longer periods than an environment with only low-level shear.

To further examine the potential importance of a mid- to upper-level shear layer, a simulation with no shear in the lowest 2.5 km and a shear layer with 10 m s^{-1} of shear per 5 km between 2.5 and 10 km is compared to the simulation with a shear of 17.5 m s^{-1} over 0–2.5 km and no shear aloft (Fig. 19c). The environment with no low-level shear fails to develop sustainable convection for the first few hours, unlike the environment with moderate low-level shear, in which the updrafts are intense over this period. This shows that low-level shear certainly is important to the initial strength of the convection. At 2.5 h, convection in the no low-level shear case redevelops along the outflow from the initial cells and grows stronger with time out to about 5 h. This behavior is very similar to the behavior of the developing convective line from the MM5 simulation. After this time, the maximum updrafts of the two simulations in Fig. 19c are very similar in magnitude. However, an important difference is seen when comparing the structure of the two solutions (not shown). After about 5 h, the simulation with no mid- to upper-level shear is no longer a squall line, but merely a propagating density current. The simulation with no low-level shear and mid- to upper-level shear continues to show upshear-tilted, deep convection along the cold pool out to 8 h, despite nearly identical values of maximum ascent along the cold pool. This again highlights that shear above the cold pool depth appears to play a role in maintaining squall line structures over longer periods than produced by low-level shear only.

These results indicate that both low-level and upper-level shear in the initial environment are important factors in both squall line strength and longevity. Admittedly, these sensitivity results need to be further examined in a 3D setting since simulated convection within strong, deep shear shows a tendency to split into isolated cells (Weisman and Klemp 1984; WKR88). Nonetheless, the present 2D simulations strengthen our presumption that upper-tropospheric shear is an important factor and should be examined further within a variety of physical frameworks in order to better understand and forecast progressive derecho events.

5. Summary and discussion

The progressive derecho is a long-lived, bowing squall line that produces large areas of damaging straight-line winds at the surface. To further our understanding of derechos and squall line longevity, a cumulonimbus-resolving model simulation of a strong, asymmetric (bowing) squall line that produces long swaths of strong winds at the lowest model layer is examined. One unique aspect of this study is that the initial and boundary conditions for the model simulation are constructed from a composite analysis of 12 warm season derecho events that occurred in association with weak large-scale forcing for upward motion. These initial conditions successfully capture the mean, large-scale environmental features that are often associated with progressive derecho events, including strong upper-level winds, relatively dry midlevels, and significant low-level warm advection. The simulated derecho is compared to previous, idealized simulations produced within horizontally homogeneous environments that have been used to explain the strength and structure of observed long-lived squall lines and bow echoes.

Rotunno et al. (1990) state that the local balance theory of RKW88 is an attempt to determine what is needed for a group of cells to develop into a strong, long-lived system and conclude that an appropriate balance between the low-level shear and the cold pool is ''a necessary (clearly not a sufficient) requirement for sustaining most strong squall lines'' (p. 1033). Analysis of the local vorticity balance terms from our simulation indicates that the squall line environment is significantly less than optimal and remains so throughout the simulation, even when considering the effects of relative flow within the cold pool. Under these conditions of local balance theory, the convective system is expected to rapidly tilt in the upshear direction and become progressively weaker with time as the strong negative vortex created baroclinically by the cold pool overwhelms the ambient shear and the cold pool surges downshear ahead of the updrafts. These expectations are based on idealized simulations in which the wind shear is restricted to the lower troposphere.

The model simulation examined in this study, which has shear throughout the depth of the troposphere and a 0–2.5- (0–5-) km shear vector magnitude of only 10–11 (15–16) m s^{-1}, produces a rapidly moving curved squall line with embedded bow echoes and severe near-surface winds for over 8 h, in which the strength of the line is maintained over a much longer period than the simulations presented in RKW88, WKR88, and W93 with similar low-level shear. More specifically, intense convective updrafts persist in the mid- and upper levels directly above the gust front for many hours, despite a significantly less than optimal condition. While these updrafts have an upshear tilt in accordance with suboptimal conditions, the updrafts maintain a nearly constant tilt for 6 h as the gust front remains nearly aligned

with the updrafts. Examination of the maximum vertical velocity and the distribution of CAPE suggests that the updrafts are not being depleted of their energy by the cold pool and that the weakening of the system is controlled more by the decrease in CAPE. A simple sensitivity test in which the CAPE along the path of the convective system is artificially increased results in a much stronger convective line with intense updrafts over the entire simulation period, even though the balance conditions remain less than optimal, which helps support this claim. Admittedly, we are not able to fully evaluate local balance theory with the MM5 simulation *in terms of its strength alone* because the intensity of the convective line may change with varying low-level shears. However, these results show that local balance theory, which only considers the importance of low-level shear, cannot explain how the strength of the simulated squall line is maintained over such a long period.

One factor that is not included in local balance theory is upper-level wind shear. The results of Lafore and Moncrieff (1989, 1990), GT92, Shapiro (1992), and Xue (2000) illustrate the importance of deep-tropospheric wind shear to squall line strength and longevity. It is interesting that the most significant difference in environments between our simulation and the previous, idealized studies is the existence of shear throughout the depth of the troposphere that results from an initial, three-dimensional environment typical of progressive derecho events. In our study, tests with a simple two-dimensional cloud-scale model indicate that low-level shear is important to the strength of the system in the first few hours of the simulation. However, these same two-dimensional simulations also show that upper-tropospheric shear (above 5 km) can significantly alter the results. While we cannot disregard the importance of a low-level vorticity balance on the basis of squall line strength alone, *these results suggest that upper-level shear can play a significant role in maintaining the strength of simulated squall lines over long periods.* Since a progressive derecho event is defined by its propensity to produce severe weather over many hours, the processes by which the initial strength of the convective line is maintained over long periods are of primary importance. These processes rendered within deep-shear environments may not be related to those proposed to determined the strength and structure of squall lines over the first few hours of their lifetime. This highlights the need to explore a wider range of environmental conditions in numerical studies of long-lived convective lines, with the hope that this more complete analysis will lead to improved conceptual models that will better assist in the forecasting of these events.

Acknowledgments. This project was partially funded by NOAA and by NSF under Grant ATM 9424397. We thank Drs. Alan Shapiro, Fred Carr, Mike Richman, and Lance Bosart for their helpful comments and suggestions. We also thank Bob Johns for many enlightening discussions. The effort of Dr. Lou Wicker in helping us with the COMMAS model is greatly appreciated. Finally, we appreciate the time and effort put forth by Dr. Morris Weisman and three anonymous reviewers, whose comments greatly improved this manuscript.

REFERENCES

Barlow, W., 1996: An examination of the Kansas derecho on 1 July 1994. Preprints, *18th Conf. on Severe Local Storms,* San Francisco, CA, Amer. Meteor. Soc., 527–530.

Barnes, S. L., 1973: Mesoscale objective map analysis using weighted time series observations. NOAA Tech. Memo. ERL NSSL-62, 60 pp. [NTIS COM-73-10781.]

Benjamin, J. B., 1968: Gravity current and related phenomena. *J. Fluid Mech.,* **31,** 209–248.

Bentley, M. L., and S. R. Cooper, 1997: The 8 and 9 July 1993 Nebraska derecho: An observational study and comparison to the climatology of related mesoscale convective systems. *Wea. Forecasting,* **12,** 673–683.

——, and T. L. Mote, 1998: A climatology of derecho-producing mesoscale convective systems in the central and eastern United States, 1986–1995. Part I: Temporal and spatial distribution. *Bull. Amer. Meteor. Soc.,* **79,** 2527–2540.

——, ——, and S. F. Byrd, 1998: A synoptic climatology of derecho-producing mesoscale convective systems: 1986–1995. Preprints, *19th Conf. on Severe Local Storms,* Minneapolis, MN, Amer. Meteor. Soc., 5–8.

Bluestein, H. B., and M. H. Jain, 1985: Formation of mesoscale lines of precipitation: Severe squall lines in Oklahoma during the spring. *J. Atmos. Sci.,* **42,** 1711–1732.

Burgess, D. W., and B. F. Smull, 1990: Doppler radar observations of a bow echo associated with a long-track severe windstorm. Preprints, *16th Conf. on Severe Local Storms,* Kananaskis Park, AB, Canada, Amer. Meteor. Soc., 203–208.

Carpenter, R. L., Jr., K. K. Droegemeier, and A. M. Blyth, 1998: Entrainment and detrainment in numerically simulated cumulus congestus clouds. Part I: General results. *J. Atmos. Sci.,* **55,** 3417–3432.

Dudhia, J., 1993: A nonhydrostatic version of the Penn State–NCAR mesoscale model: Validation tests and simulation of an Atlantic cyclone and cold front. *Mon. Wea. Rev.,* **121,** 1493–1513.

Evans, J. S., and C. A. Doswell III, 1998: An examination of observed shear profiles associated with long-lived bow echoes. Preprints, *19th Conf. on Severe Local Storms,* Minneapolis, MN, Amer. Meteor. Soc., 30–33.

——, and ——, 2001: Examination of derecho environments using proximity soundings. *Wea. Forecasting,* **16,** 329–342.

Fovell, R. G., and Y. Ogura, 1988: Numerical simulation of a midlatitude squall line in two dimensions. *J. Atmos. Sci.,* **45,** 3846–3879.

Fujita, T. T., 1955: Results of detailed synoptic studies of squall lines. *Tellus,* **7,** 405–435.

——, 1976: Spearhead echo and downburst near the approach end of a John F. Kennedy Airport runway, New York City. SMRP Research Paper 137, University of Chicago, 51 pp.

——, 1978: Manual of downburst identification for Project NIMROD. SMRP Research Paper 156, University of Chicago, 104 pp.

——, 1981: Tornadoes and downbursts in the context of generalized planetary scales. *J. Atmos. Sci.,* **38,** 1512–1534.

——, and R. M. Wakimoto, 1981: Five scales of airflow associated with a series of downbursts on 16 July 1980. *Mon. Wea. Rev.,* **109,** 1438–1456.

Garner, S. J., and A. J. Thorpe, 1992: The development of organized convection in a simplified squall-line model. *Quart J. Roy. Meteor. Soc.,* **118,** 101–124.

Goff, R. C., 1976: Vertical structure of thunderstorm outflows. *Mon. Wea. Rev.,* **104,** 1429–1440.

Hamilton, R. E., 1970: Use of detailed intensity radar data in me-

soscale surface analyses of the 4 July 1969 storm in Ohio. Preprints, *14th Conf. on Radar Meteorology*, Tucson, AZ, Amer. Meteor. Soc., 339–342.

Hinrichs, G., 1888: Tornadoes and derechos. *Amer. Meteor. J.,* **5,** 306–317, 341–349.

Houze, R. A., Jr., S. A. Rutledge, M. I. Biggerstaff, and B. F. Smull, 1989: Interpretation of Doppler weather radar displays of midlatitude mesoscale convective systems. *Bull. Amer. Meteor. Soc.,* **70,** 608–619.

Johns, R. H., 1984: A synoptic climatology of northwest flow severe weather outbreaks. Part II: Meteorological parameters and synoptic patterns. *Mon. Wea. Rev.,* **112,** 449–464.

——, 1993: Meteorological conditions associated with bow echo development in convective storms. *Wea. Forecasting,* **8,** 294–299.

——, and W. D. Hirt, 1985: The derecho of 19–20 July 1983. . . A case study. *Natl. Wea. Dig.,* **10,** 17–32.

——, ——, 1987: Derechos: Widespread convectively induced windstorms. *Wea. Forecasting,* **2,** 32–49.

——, and P. J. Leftwich, 1988: The severe thunderstorm outbreak of 28–29 July 1986. A case exhibiting both isolated supercells and a derecho-producing convective system. Preprints, *15th Conf. on Severe Local Storms,* Baltimore, MD, Amer. Meteor. Soc., 448–451.

——, and C. A. Doswell III, 1992: Severe local storms forecasting. *Wea. Forecasting,* **7,** 588–612.

——, K. W. Howard, and R. A. Maddox, 1990: Conditions associated with long-lived derechos—An examination of the large-scale environment. Preprints, *16th Conf. on Severe Local Storms,* Kananaskis Park, AB, Canada, Amer. Meteor. Soc., 408–412.

Johnson, R. H., and P. J. Hamilton, 1988: The relationship of surface pressure features to the precipitation and airflow structure of an intense midlatitude squall line. *Mon. Wea. Rev.,* **116,** 1444–1463.

Jorgensen, D. P., and B. F. Smull, 1993: Mesovortex circulations seen by airborne Doppler radar within a bow-echo mesoscale convective system. *Bull. Amer. Meteor. Soc.,* **74,** 2146–2157.

Kain, J. S., and J. M. Fritsch, 1993: Convective parameterization for mesoscale models: The Kain–Fritsch scheme. *The Representation of Cumulus Convective in Mesoscale Numerical Models, Meteor. Monogr.,* No. 46, Amer. Meteor. Soc., 165–170.

——, and ——, 1998: Multiscale convective overturning in mesoscale convective systems: Reconciling observations, simulations, and theory. *Mon. Wea. Rev.,* **126,** 2254–2273.

Klemp, J. B., and R. B. Wilhelmson, 1978: The simulation of three-dimensional convective storm dynamics. *J. Atmos. Sci.,* **35,** 1070–1096.

Lafore, J., and M. W. Moncrieff, 1989: A numerical investigation of the organization and interaction of the convective and stratiform region of tropical squall lines. *J. Atmos. Sci.,* **46,** 521–544.

——, and ——, 1990: Reply. *J. Atmos. Sci.,* **47,** 1034–1036.

Maddox, R. A., 1980a: Mesoscale convective complexes. *Bull. Amer. Meteor. Soc.,* **61,** 1374–1387.

——, 1980b: An objective technique for separating macroscale and mesoscale features in meteorological data. *Mon. Wea. Rev.,* **108,** 1108–1121.

——, 1983: Large-scale conditions associated with midlatitude, mesoscale convective complexes. *Mon. Wea. Rev.,* **111,** 1475–1493.

Moncrieff, M. W., 1992: Organized convective systems: Archetypal dynamical models, mass and momentum flux theory, and parameterization. *Quart. J. Roy. Meteor. Soc.,* **118,** 819–850.

——, and C. Liu, 1999: Convection initiation by density currents: Role of convergence, shear, and dynamical organization. *Mon. Wea. Rev.,* **127,** 2455–2464.

Munoz, L. A., and R. B. Wilhelmson, 1993: Structure and evolution of thunderstorms encountering temperature inversions. Preprints, *17th Conf. on Severe Local Storms,* St. Louis, MO, Amer. Meteor. Soc., 247–251.

Nolan, R. H., 1959: A radar pattern associated with tornadoes. *Bull. Amer. Meteor. Soc.,* **40,** 277–279.

Orlanski, I., 1975: A rational sub-division of scales for atmospheric processes. *Bull. Amer. Meteor. Soc.,* **56,** 527–530.

Przybylinski, R. W., 1995: The bow echo: Observations, numerical simulations, and severe weather detection methods. *Wea. Forecasting,* **10,** 203–218.

——, and D. M. DeCaire, 1985: Radar signatures associated with the derecho, a type of mesoscale convective system. Preprints, *14th Conf. on Severe Local Storms,* Indianapolis, IN, Amer. Meteor. Soc., 228–231.

Rotunno, R., J. B. Klemp, and M. L. Weisman, 1988: A theory for strong, long-lived squall lines. *J. Atmos. Sci.,* **45,** 463–485.

——, ——, and ——,1990: Comments on ''A numerical investigation of the organization and interaction of the convective and stratiform region of tropical squall lines.'' *J. Atmos. Sci.,* **47,** 1031–1033.

Schmidt, J. M., and W. R. Cotton, 1989: A high plains squall lines associated with severe surface winds. *J. Atmos. Sci.,* **46,** 281–302.

Seitter, K. L., 1986: A numerical study of atmospheric density current motion including the effects of condensation. *J. Atmos. Sci.,* **43,** 3068–3076.

Shapiro, A., 1992: A hydrodynamical model of shear flow over semi-infinite barriers with application to density currents. *J. Atmos. Sci.,* **49,** 2293–2305.

Simpson, J. E., and R. E. Britter, 1980: A laboratory model of an atmospheric mesofront. *Quart. J. Roy. Meteor. Soc.,* **106,** 485–500.

Skamarock, W. C., M. L. Weisman, and J. B. Klemp, 1994: Three-dimensional evolution of simulated long-lived squall lines. *J. Atmos. Sci.,* **51,** 2563–2584.

Smull, B. R., and R. A. Houze Jr.,1987: Rear inflow in squall lines with trailing stratiform precipitation. *Mon. Wea. Rev.,* **115,** 2869–2889.

Thorpe, A. J., M. J. Miller, and M. W. Moncrieff, 1982: Two-dimensional convection in non-constant shear: A model of mid-latitude squall lines. *Quart. J. Roy. Meteor. Soc.,* **108,** 739–760.

Wakimoto, R. M., 1982: The life cycle of thunderstorm gust fronts as viewed with Doppler radar and rawinsonde data. *Mon. Wea. Rev.,* **110,** 1060–1082.

Weisman, M. L., 1992: The role of convectively generated rear-inflow-jets on the evolution of long-lived mesoconvective systems. *J. Atmos. Sci.,* **49,** 1826–1847.

——, 1993: The genesis of severe, long-lived bow echoes. *J. Atmos. Sci.,* **50,** 645–670.

——, and J. B. Klemp, 1984: The structure and classification of numerically simulated convective storms in directionally varying wind shears. *Mon. Wea. Rev.,* **112,** 2479–2498.

——, and C. A. Davis, 1998: Mechanisms for the generation of mesoscale vorticies within quasi-linear convective systems. *J. Atmos. Sci.,* **55,** 2603–2622.

——, J. B. Klemp, and R. Rotunno, 1988: Structure and evolution of numerically simulated squall lines. *J. Atmos. Sci.,* **45,** 1990–2013.

——, W. C. Skamarock, and J. B. Klemp, 1997: The resolution dependence of explicitly modeled convective systems. *Mon. Wea. Rev.,* **125,** 527–546.

Wicker, L. J., and R. B. Wilhelmson, 1995: Simulation and analysis of tornado development and decay within a three-dimensional supercell thunderstorm. *J. Atmos. Sci.,* **52,** 2675–2703.

Xue, M., 2000: Density currents in two-layer shear flows. *Quart. J. Roy. Atmos. Sci.,* **126,** 1301–1320.

Zhang, D. L., 1989: The effect of parameterized ice microphysics on the simulation of a vortex circulation with a mesoscale hydrostatic model. *Tellus,* **41A,** 132–147.

——, and R. A. Anthes, 1982: A high-resolution model of the planetary boundary layer—sensitivity tests and comparisons with SESAME-79 data. *J. Appl. Meteor.,* **21,** 1594–1609.